Mechanical Shielding in Plant Nuclei

Rituparna Goswami, Atef Asnacios, Pascale Milani, Stéfanie Graindorge, Guy Houlné, Jérôme Mutterer, Olivier Hamant, Marie-Edith Chabouté

▶ **To cite this version:**

Rituparna Goswami, Atef Asnacios, Pascale Milani, Stéfanie Graindorge, Guy Houlné, et al.. Mechanical Shielding in Plant Nuclei. Current Biology - CB, 2020, 30 (11), pp.2013-+. 10.1016/j.cub.2020.03.059 . hal-02993638

HAL Id: hal-02993638
https://hal.science/hal-02993638

Submitted on 16 Nov 2020

HAL is a multi-disciplinary open access archive for the deposit and dissemination of scientific research documents, whether they are published or not. The documents may come from teaching and research institutions in France or abroad, or from public or private research centers.

L'archive ouverte pluridisciplinaire **HAL**, est destinée au dépôt et à la diffusion de documents scientifiques de niveau recherche, publiés ou non, émanant des établissements d'enseignement et de recherche français ou étrangers, des laboratoires publics ou privés.

Click here to access/download;Graphical Abstract;GraphAbstractRev21March.tif

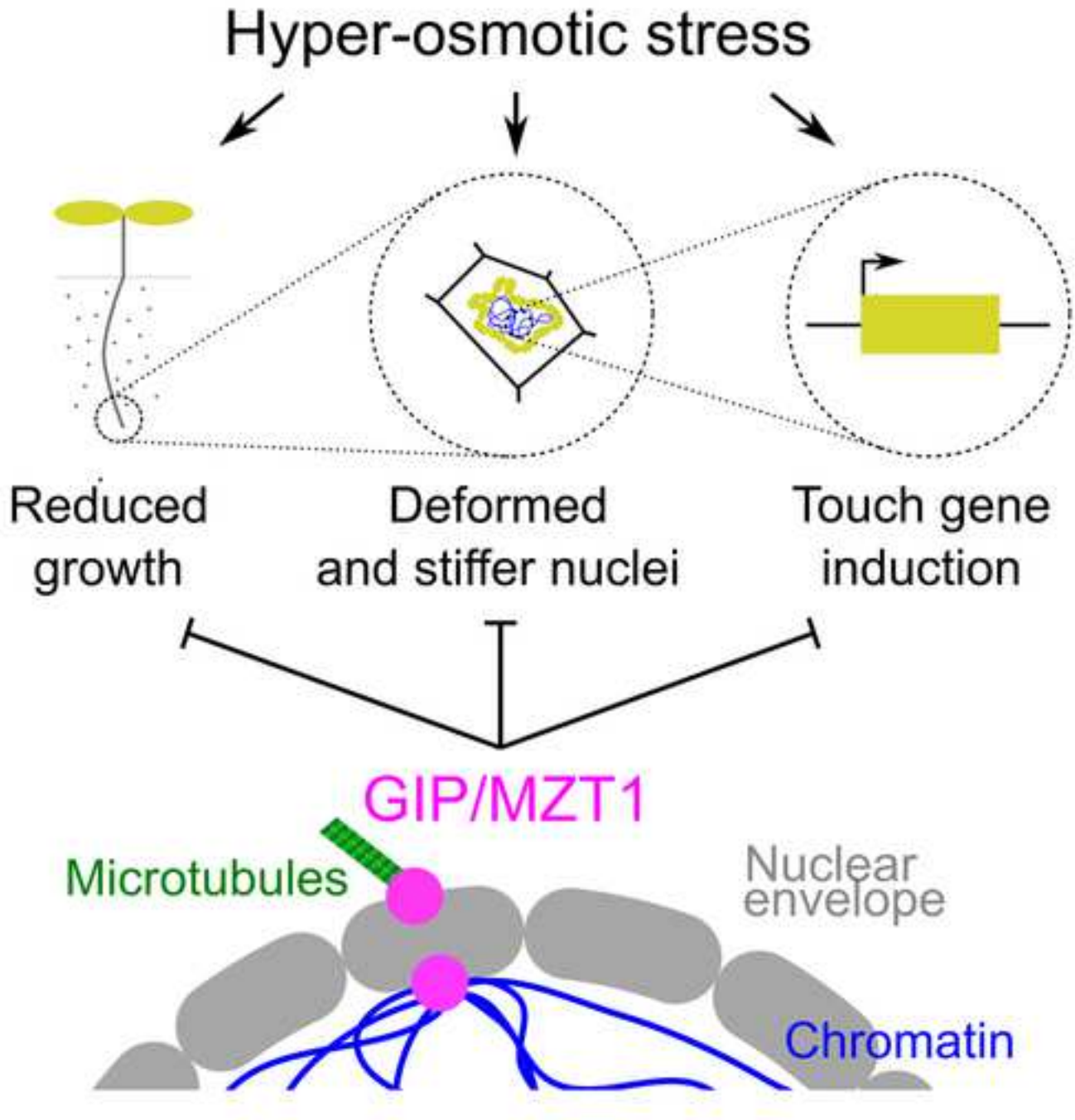

Mechanical shielding in plant nuclei

Rituparna Goswami[a,b], Atef Asnacios[c], Pascale Milani[d], Stéfanie Graindorge[a], Guy Houlné[a], J. Mutterer[a], Olivier Hamant[b*] and Marie-Edith Chabouté[a1*]

[a] Institut de biologie moléculaire des plantes, CNRS, Université de Strasbourg, 67084 Strasbourg, France

[b] Laboratoire de Reproduction et Développement des Plantes, Université de Lyon, UCB Lyon 1, ENS de Lyon, INRAE, CNRS, 69364 Lyon, France

[c] Laboratoire Matières et Systèmes Complexes, Université de Paris, CNRS, Université Paris-Diderot, 75013 Paris, France

[d] BioMéca, ENS de Lyon, 69364 Lyon, France

*Correspondence: marie-edith.chaboute@ibmp-cnrs.unistra.fr ; olivier.hamant@ens-lyon.fr

[1] Lead contact

Summary

In animal single cells in culture, nuclear geometry and stiffness can be affected by mechanical cues, with important consequences for chromatin status and gene expression. This calls for additional investigation into the corresponding physiological relevance in a multicellular context and in different mechanical environments. Using the Arabidopsis root as a model system, and combining morphometry and micro-rheometry, we found that hyperosmotic stress decreases nuclear circularity and size and increases nuclear stiffness in meristematic cells. These changes were accompanied by enhanced expression of touch response genes. The nuclear response to hyperosmotic stress was rescued upon return to iso-osmotic conditions, and could even lead to opposite trends upon hypo-osmotic stress. Interestingly, nuclei in a mutant impaired in the functions of GIP/MZT1 proteins at the nuclear envelope, were almost insensitive to such osmotic changes. The *gip1gip2* mutant exhibited constitutive hyperosmotic stress response with stiffer and deformed nuclei, as well as touch response gene induction. The mutant was also resistant to lethal hyperosmotic conditions. Altogether we unravel a stereotypical geometric, mechanical and genetic nuclear response to hyperosmotic stress in plants. Our data also suggest that chromatin acts as a viscous elastic gel that stiffens in hypertonic conditions, and that the nuclear envelope-associated protein GIPs act as negative regulators of this response.

Keywords: Nuclear mechanics; micro-rheometry; AFM; nuclear shape; nuclear envelope; hyperosmotic stress; touch gene; Arabidopsis; root tip; GIP/MZT1

Introduction

All living organisms are able to sense and respond to mechanical forces during their development [1]. Typically in animal cells, mechanical stress affects the cytoskeleton at the cell cortex [2]. Mechanical stress also has intracellular effects on nuclear shape and stiffness [3,4] and this may ultimately impact 3D chromatin organization and gene expression [5–8].This either implies propagation of mechanical signals through the nucleus via biochemical cascades or more directly, through the LINC complexes at the nuclear envelope, at the nexus between cytoskeleton and nucleoskeleton [9–11]. Thus the stress born by the cytoskeleton can be transmitted to the nucleoskeleton, composed of lamins, and to chromatin [12–14]. Changes in tension levels at the nuclear envelope can also impact the entry of transcription factors [15] Yet, the interplay between nuclear shape and stiffness, and its contribution to nuclear function, is still not fully understood in animals [16–18] and is completely unknown in plants.

Mechanical stress can be induced by changing osmotic conditions, through modification of the internal hydrostatic pressure that affects the cell cortex [19]. Thus, the role of membrane tension in cell polarity can be revealed by modifying the osmolarity of the medium in which single cells in culture are kept [20]. Hyperosmotic stress was also shown to shrink the nucleus through an uneven distribution of macromolecules between cytoplasm and nucleoplasm [21] and to affect gene expression by modifying chromatin compaction [3]. Under natural conditions, high salinity and drought are the most frequent causes of osmotic stress in plants [22]. Osmotic stress leads to changes in chromatin remodeling and gene expression to protect the cell [23–25].

As in animals, gene expression in plants is in part under mechanical control. For instance, the expression of 2.5% of the genome is significantly affected by a gentle touch in Arabidopsis [26,27]. Furthermore, the expression of the transcription factor *PtaZFP2* linearly correlates with stem bending in poplar [28], and the expression level of homeodomain master regulator SHOOT MERISTEMLESS scales to tissue folding and can be induced by mechanical perturbation during organogenesis at the shoot apical meristem [29]. Yet, whether osmotic conditions affect nuclear mechanics and shape, and whether gene expression relates to such modifications is unknown.

Variation in nuclear shape is observed in mutants impaired in LINC components or in plant-specific proteins found at the nuclear envelope. Among them are the plant functional

homologs of lamins (KAKU4, NEAP, CRWN1-4) [30–33], as well as human MZT1 homologs, GCP3 interacting proteins (GIP) 1 and 2 [34]. GIP1 and GIP2 are associated to microtubule nucleation complexes via the gamma-tubulin protein complex3 (GCP3) [35,36]. Later on, they were also found to be associated to centromeric chromatin [34,37] (see Figure 2A). Here we explore the relation between nuclear stiffness and morphology in the multicellular context of the Arabidopsis root tip. Combining hyperosmotic stress, *gip1gip2* mutations, nuclear shape and micro-rheometric measurements, as well as RNAseq analysis, we show that nuclear stiffness and touch gene expression scale with the osmotic environment of the cell. In addition, we show that plants defective in GIP proteins exhibit this response constitutively, correlating with an increased ability of the plant to resist hyperosmotic stress.

Results

Hyperosmotic stress decreases nuclear circularity and size in root tip cells

Building on results obtained in animal cells where osmotic stress affects nuclear shape [21], we tested the nuclear response to hyperosmotic stress in Arabidopsis root tips. Nine-day-old Arabidopsis seedlings expressing the inner nuclear membranuclear envelope SUN1-GFP marker [38] were exposed to 0.3 M mannitol for 16 hours (Figure 1). Nuclear shape was analysed by confocal microscopy, focusing on the central part of the root meristem and the external layers of the root (epidermis and cortex, see white frames in Figures 1A and 1B). Whereas most nuclei displayed round shapes in untreated seedlings, the treated nuclei exhibited irregular shapes and reduced size that were further quantified (Figures 1A-1B).
Nuclear circularity was equal to 0.93 ± 0.001 in control seedlings, (n = 99), and 0.85 ± 0.008 in treated seedlings (n = 98), which is significantly different from the control (*p*-value = 3.23e-16, Figure 1C). Nuclear area reached 75% of its initial area, from 41.1 ± 0.75 μm^2 in untreated seedlings to 32.1 ± 1 μm^2 in treaded seedlings (*p*-value = 1.63e-11, Figure 1E). Similar findings were observed when considering the 3D nature of the nuclei (see method details): nuclear sphericity decreased from 0.59 ± 0.008 in control plants (n = 20) to 0.53 ± 0.01 in treated plants (n = 20, *p*-value = 0.0006, Figure 1D); upon hyper-osmotic stress, nuclear volume reached 71% of its initial volume (n = 20, *p*-value = 0.0001, Figure 1F). As the trends in 2D and 3D are comparable, and because 3D measurements are more difficult to extract in our confocal microscopy set-up, we mainly focused our analysis on 2D measurements in the following.

Interestingly, under lower osmotic stress conditions, *i.e.* 0.15 M mannitol, no nuclear deformation could be detected in root meristems indicating the presence of a threshold in the response ($n_{control}$ = 54, $n_{treated}$ = 68, *p*-values = 0.16 and 0.17 for nuclear circularity and area respectively, Figures S1A-S1D). To confirm that the response is not mannitol specific, we also tested another osmolyte. A 0.15 M NaCl treatment, similar in osmolarity to 0.3 M mannitol, induced a decrease in nuclear circularity and area comparable to what observed with 0.3 M mannitol (circularity of 0.84 ± 0.01 and area of 31.95 ± 1.75 μm^2 after treatment, $n_{control}$ = 91, $n_{treated}$ = 51, *p*-values = 1.98e-8 and 0.0043 respectively, Figures S1E-S1H).
In order to see if changes in nuclear geometry could reflect changes in cell shape [39], we analyze cytoplasmic detachment from the cell wall in our root meristem under hyperosmotic

stress (0.3M mannitol). This effect was mild and the overall cell shape was not modified (Figures S1I-S1K, see white arrows in J, K). As the impact on the nucleus is in contrast severe, the nucleocytoplasmic volume ratio decreased significantly from 0.25 ± 0.01 to 0.19 ± 0.008 (n = 20, *p*-value = 0.0022), while the cell volume remained unchanged (*p*-value = 0.19, Figures 1G and 1H). Altogether, this demonstrates that hyperosmotic shock in root meristems decreases nuclear circularity and area, without significantly changing cell volume.

Nuclear shape defects in *gip1gip2* mimic hyperosmotic stress

The *gip1gip2* knocked-down mutant is impaired in the recruitment of microtubule nucleation complexes and centromeric chromatin architecture leading to ploidy defects [36,37] (Figure 2A). The mutant also exhibits severe developmental defects. Root growth is altered, and is variable from mild to strong phenotype (Figure S2A). As previously shown, root meristem nuclei from *gip1gip2* SUN1-GFP seedlings exhibit shape defects [34] (Figure 2B) that resemble that of wild-type (WT) nuclei under hyperosmotic stress (Figure 1B). To go beyond this qualitative comparison, we characterized the nuclear shape of the mutant. Nuclear circularity in *gip1gip2* was equal to 0.78 ± 0.013 (n = 74, Figure 2D), which was significantly lower than the untreated WT (0.93 ± 0.001, n = 99, *p*-value = 2.19e-26, see Figure 1C). However, nuclear area was increased in *gip1gip2* and reached 63.8 ± 3.45 μm^2 on average (n = 74, Figure 2E), to compare to 41.1 ± 0.75 μm^2 in untreated WT (n = 99, *p*-value = 9.79e-12, see Figure 1D). Increased average nuclear area may relate to increased ploidy levels in the mutant [36,37]. In order to compare nuclear area between WT and mutant independent of ploidy, we analysed the area of WT and *gip1gip2* nuclei in 2C flow-sorted root nuclei. This revealed that 2C *gip1gip2* nuclei exhibit significantly smaller nuclei when compared to WT nuclei ($n\ 2C_{WT}$ = 18 and $n\ 2C_{gip1gip2}$ = 19, *p*-value = 0.0014, Figure S2F). This demonstrates that *gip1gip2* has more compact nuclei than the WT nuclei. This confirms that *gip1gip2* nuclei fully mimic WT nuclei under hyperosmotic stress, at least from a geometric standpoint.

Next, we investigated whether hyperosmotic stress could aggravate the *gip1gip2* phenotype. To do so, we treated *gip1gip2* seedlings with 0.3 M mannitol, as shown above for the WT. In such conditions, no more deformation was observed in *gip1gip2* nuclei (Figures 2B and 2C): nuclear circularity (0.74 ± 0.017; n = 45) and nuclear area (62.8 ± 5.53 μm^2; n = 45) were not significantly different from the untreated *gip1gip2* control (0.78 ± 0.013 and 63.8 ± 3.45 μm^2 respectively, n = 74, *p*-values = 0.118 and 0.875, respectively, Figures 2D and 2E). Note that

we reached the same conclusions when analysing *gip1gip2* seedlings with milder phenotypes (Figures S2B-S2E). Altogether, these results suggest that *gip1gip2* may constitutively activate a hyperosmotic response.

gip1gip2 mutants resist to high hyperosmotic stress

If the *gip1gip2* mutant nuclei already exhibit a hyperosmotic-like response, this may also prime the plant to resist to hyperosmotic conditions. In order to test that hypothesis, we analysed the mutant phenotype upon 0.4 M and 0.6 M mannitol treatment. In these severe hyperosmotic conditions, widespread cell death occurred in WT root meristems (Figures 3A and 3B). In contrast, most of the *gip1gip2* root tip cells from seedlings exhibiting a mild phenotype survived the treatment (Figures 3A and 3B).

In the surviving WT cells, nuclei were strongly deformed upon treatment with 0.4 and 0.6 M mannitol, when compared to iso-osmotic control ($n_{control} = 38$, $n_{0.4\ M} = 39$, $n_{0.6\ M} = 41$, *p*-values for control vs. 0.4 M and control vs. 0.6 M are 2.903e-9, 1.51e-6 and 1.60e-10, 3.58e-10 for nuclear circularity and area, respectively, Figures 3C and 3D). Furthermore, when compared to 0.3 M mannitol (Figures 1C and 1E), nuclear circularity was even more reduced at 0.4 M mannitol (*p*-value = 0.038) while the nuclear area was lower at 0.6 M mannitol (*p*-value = 0.019). No significant differences were observed between 0.4 M and 0.6 M mannitol (*p*-values = 0.094 and 0.075, respectively for nuclear circularity and area, Figures 3C and 3D). This indicates a threshold in the response to hyperosmotic stress for the WT. In contrast, the *gip1gip2* nuclear shapes remained unchanged in these harsher osmotic conditions ($n_{control} = 58$, $n_{0.4\ M} = 22$, $n_{0.6\ M} = 43$; *p*-values, control vs. 0.4 M and control vs. 0.6 M, are 0.33, 0.61 and 0.99, 0.53 for nuclear circularity and area, respectively, Figures 3E and 3F). This suggests that a maximum of nuclei deformation exists in the WT, and that *gip1gip2* already reaches it in control conditions.

To test how the *gip1gip2* mutant root grows in such harsh osmotic conditions, we analysed the impact of such conditions on root length in the WT and mutant. Nine-day-old seedlings were grown in normal conditions and then transferred on 0.4 M and 0.6 M mannitol for 2 days. In the WT, final root length was decreased by a factor 5 after transfer to 0.4 M (n =13, *p*-value 3.8e-7) and by a factor 18.2 after transfer to 0.6 M mannitol (n = 12, *p*-value = 3.54e-5, Figure 3G). Although we also saw an impact on root length in *gip1gip2*, this was much milder: final *gip1gip2* root length was decreased by a factor 2 after transfer to 0.4 M (n = 10,

p-value = 0.0029) and by a factor 4.4 after transfer to 0.6 M mannitol (n = 13, *p*-value = 1.74e-6 Figure 3G, Figure S3A). Note that the *gip1gip2* mutant also seemed to resist to such harsh conditions even in the long term: after 15 days in harsh osmotic conditions, the *gip1gip2* exhibited reduced leaf senescence when compared to the WT (n = 14, Figures 3H and 3I).

Next, we measured root growth for 5 days in our standard hyperosmotic conditions (0.3 M mannitol) using WT as well as mild and severe *gip1gip2* mutants. As expected, in these conditions, root growth was dramatically reduced in the WT (Figure 3J). In contrast, root growth was only slightly affected in the mild *gip1gip2* mutants but the difference was too small to be statistically significant ($n_{control} = 7$, $n_{treated} = 6$, *p*-value = 0.095, Figure 3I, Figure S3B). In the severe *gip1gip2* mutants, root growth was unchanged ($n_{control} = 6$, $n_{treated} = 7$, *p*-value = 0.63, Figure 3J, Figure S3B).

Altogether, we identify three nuclear responses to hyperosmotic stress in the WT: up to 0.15 M mannitol, nuclear shape is stable; at 0.3 M mannitol, nuclei shrink and become more circumvoluted; above 0.3 M mannitol, nuclei are even more deformed but cells die, consistent with growth defects under such harsh hyperosmotic conditions. Because the *gip1gip2* mutant nuclei are already more compact than the WT, this may also prime the mutant to resist hyperosmotic stress.

Nuclear deformation upon hyperosmotic stress or with defective GIPs correlates with nuclear stiffening

In theory, wavy nuclear envelope could result from cytoplasmic forces acting on a soft nucleus (in which case the cytoskeleton would shape the nucleus upon hyperosmotic stress), or from nuclear factors shaping and stiffening the nucleus (in which case, the nucleoskeleton and/or chromatin would shape the nucleus upon hyperosmotic stress). To discriminate between these two scenarios, we isolated nuclei from root meristems and checked their shape. Although extracted nuclei appeared smaller than nuclei in tissues, shape defects were still maintained in WT extracted nuclei upon mannitol treatment ($n_{control\ WT} = 33$, $n_{treated\ WT} = 57$, *p*-values = 2.7 e-9 and 0.0079 for nuclear circularity and area respectively, Figures S4A, S4B, S4E, S4F). No significant difference in area or circularity was observed in extracted *gip1gip2* nuclei after mannitol treatment ($n_{control\ gip1gip2} = 34$, $n_{treated\ gip1gip2} = 53$, *p*-values = 0.94 and 0.083 for nuclear circularity and area, respectively; Figures S4C, S4D, S4G, S4H). This

suggests that the impact of hyperosmotic stress on nuclear shape mainly depends on the nucleus itself.

This prompted us to test the intrinsic physical properties of the nucleus. To do so, we measured the stiffness of isolated nuclei from untreated and treated WT root tips. First, we adapted a micro-rheometry approach, initially developed to measure whole cell stiffness [40,41]: the nucleus is compressed between two microplates, one flexible and the other one more rigid; the stiffness of the sample is deduced from the deflection of the flexible microplate, the stiffness of which is calibrated (Figures 4A-4C, see method details). Root meristematic nuclei were isolated from 9-day-old untreated or treated seedlings using a FACS-based protocol and they were then resuspended in MS medium with or without mannitol (as in whole plant treatments, see method details). Note that nuclear envelope integrity was confirmed by the presence of SUN1-GFP and microtubules (Figures S4I and S4J). Nuclei that were resuspended in control medium exhibited an elastic modulus of 0.39 ± 0.07 kPa (n = 17, Figure 4D, video S1). In contrast, nuclei that were resuspended in hyperosmotic conditions were about 10 times stiffer (4.15 ± 1.78 kPa, n = 11, *p*-value = 0.0029, Figure 4D, video S2). This shows that reduced nuclear circularity and area upon hyperosmotic stress correlates with increased nuclear stiffness. If true, this should apply to *gip1gip2* nuclei too. Consistently, we found that *gip1gip2* mutant nuclei were also stiffer than WT nuclei (2.88 ± 1.38 kPa, n = 17, *p*-value = 0.0001, Figure 4D) and with a stiffness value comparable to that of mannitol-treated WT nuclei (4.15 ± 1.78 kPa, n = 11, *p*-value = 0.643, Figure 4D). Therefore, it seems that not only *gip1gip2* mutants mimic the effect of hyperosmotic stress observed on WT nuclear shape, but it also mimics its impact on nuclear stiffness.

To validate these results *in planta*, we used atomic force microscopy (AFM). A sharp tip is attached on a flexible cantilever, which stiffness is calibrated. The deformation of the cantilever as it contacts the sample is monitored *via* a laser beam reflecting from the top surface of the cantilever into a photodetector. This provides force–displacement curves from which the mechanical properties of the sample can be derived (Figures 4E, S4L and S4M). Nuclei from WT and *gip1gip2* root meristems from 9-day-old seedlings were analysed after *in situ* cell wall digestion and meristem squashing (Figures 4F and 4H). The cantilever was applied on the nuclei *in planta* on poly-L-Lysine coated petri dishes (Figures 4F and 4H). After acquiring matrix forces curves (Figures 4G and 4H, inset; Figures S4L and S4M),

topography and rigidity maps were obtained using the peakforce QNM (quantitative Nanomechanical mapping) mode (Figures 4G and 4I). Despite the differences in sample preparation between AFM and micro-rheometry, we found no significant preparation-dependent difference in the elastic modulus of the WT nuclei (Figure S4K), thus validating our approaches to compare the samples. Our AFM measurements confirmed the micro-rheometry analyses: nuclei from untreated WT root tips exhibited an apparent elastic modulus (Ea) of 37.4 ± 3.6 kPa whereas *gip1gip2* mutant nuclei were much stiffer, at 89.0 ± 8.3kPa (Figure 4J, n = 14, *p*-value = 0.0018). Thus, *gip1gip2* nuclei are significantly stiffer than those of the WT, whether nuclear stiffness is measured by micro-rheometry or AFM.

Altogether we show that hyperosmotic stress leads to increased nuclear stiffness, which correlates with decreased nucleus size and area. This trend is mimicked in *gip1gip2* mutants. Because nuclear shape and stiffness can affect gene expression, we next checked whether hyperosmotic stress and *gip1gip2* mutation also have consistent effects on the transcriptome.

Hyperosmotic stress and *gip1gip2* mutation induce overlapping transcriptional stress responses

First, we analysed gene expression in *gip1gip2* mutants using total RNA sequencing and RT-qPCR. We used *gip1gip2* mutant populations from 9-day-old seedlings, with either mild or strong phenotypes (Figure S2A). Using a NGS approach (Illumina), we analysed 125 bp reads. PCA analysis revealed three different groups matching plant phenotypes (DESeq2 package). This approach generated a list of the shared most up-regulated genes in mild and severe *gip1gip2*, when compared to WT (Figure S5A). A list of differentially expressed genes was then selected with z-score calculations using Benjamini Hochberg corrections of 0.05 for false-discovery rate. The *gip1gip2* mutant displayed major deviations from the WT in stress response genes, as annotated through their Gene Ontology (Table S1). In particular, the *gip1gip2* transcriptome shared 57% of the transcripts identified in the transcriptome of touched plants [26], with a statistical significance of the overlap (Representation factor R = 7.8 with a probability p < 4.661e-231 using hypergeometric test, Figure 5A).

Conversely, a significant overlap with the transcriptome of *gip1gip2* was obtained when considering WT seedlings treated with high concentration of mannitol (21.4% of overlapping transcripts) or high concentration of sodium chloride (28.6 % of overlapping transcripts)

(Figures S5B and S5C, R=3.9 and 2.9 respectively and an exact hypergeometric probability p < 2.904e-118, [42].

Among the most up-regulated touch response genes (76 genes), 60 were also up-regulated in *gip1gip2*. To check whether this response is specific to GIP, we analysed the expression of these genes in the transcriptomic data of another nuclear envelope mutant, *cpr5*. This nucleoporin mutant exhibits major defects in nuclear shape and plant development [43]. Yet, although 23.6 % of the transcriptome of *cpr5* overlapped with that of *gip1gip2* (Figure S5D, R= 3.2 with a p < 9.70e-57, using hypergeometric test), only 7 genes were found to overlap with the most up-regulated touch response genes. This suggests that the GIP-dependent nuclear deformation and gene expression profile exhibits some degree of specificity, with a more prominent link to mechanical stress.

Then, we focused our analysis on a subset of 18 touch response genes, based on their established induction in response to mechanical perturbations [26,44] such as the *TOUCH* gene family (Figure S5E). First, we validated the expression of the selected 18 genes using RT-qPCR (Figure 5B). RT-qPCR was performed on 9-day-old *gip1gip2* and WT seedlings using specific primers for the 18 selected genes (Table S2). As expected, we found a significantly increased transcript levels in *gip1gip2* for these 18 genes. The induction was also stronger in the severe *gip1gip2* mutant than in the mild one (Figure S5E). More specifically, mechanosensitive genes such as *TCH2*, *TCH3*, *TCH4*, *WRKY33*, *WRKY40*, *CPK28*, *CPK32*, *Calcium-binding EF-hand gene*, *AT1G76600*, *DREB26*, *NHL3*, *HSPRO2* displayed 3- to 16-fold higher transcript levels in *gip1gip2*, when compared to WT (Figure 5B). The transcript level of genes encoding the Salt tolerance zinc finger, the transcription factors WRKY18, WRKY40, Myb44 and SZF1 as well as the cytochrome CYP81D8 and the AAA-type ATPase family member was even more increased, from 20- up to 120-fold in *gip1gip2* compared to WT (Figure 5B). Interestingly, none of these 18 genes were found up-regulated in *cpr5* (Figure S5E).

To check whether similar transcript level changes were observed upon hyperosmotic stress, we performed similar analyses on the 0.3 M mannitol-treated seedlings compared to control plants. Under hyperosmotic stress, 9-day-old seedlings exhibited a response comparable to that of *gip1gip2*, albeit to a lower extent with mRNA levels changing from 2.4- to 53-fold (Figure 6A). Note that similar results were also obtained when analyzing the mRNA levels in

roots only, allowing us to formally correlate nuclear deformation and transcriptional response under hyperosmotic stress in root meristematic nuclei (Figure S6A).

As we observed that 0.15M mannitol is not sufficient to induce a detectable change in nuclear shape, we also analysed gene expression in these milder conditions. As expected, under such low stress conditions (0.15 M mannitol), no significant induction could be observed for the selected genes (*i.e.*, below a 2-fold induction, Figure S6D). This further correlates changes in nuclear shape with gene expression, including the threshold in the cellular response to hyperosmotic stress.

Last, we found that most of the mechanosensitive genes were induced in the *gip1gip2* mutant upon a 0.3 M mannitol treatment, albeit to a lesser extent when compared to WT, from 0.7- to 4.3-fold change in mRNA level (Figure S6C), consistent with the observation that *gip1gip2* already exhibits a close to maximal nuclear shape deformation before mannitol treatment.

Transcriptional nuclear responses to hyperosmotic stress are reversible

If the impact of hyperosmotic stress on transcriptome is associated with nuclear mechanics, it should be reversible. To test this hypothesis, we exposed 9-day-old seedlings to hyperosmotic stress for 16 hours and then transferred them back to normal medium for 7 hours. As a control, 9-day-old seedlings were exposed to normal medium for 16 hours and then transferred to fresh normal medium for an additional 7 hours. We then analysed the expression of the 18 selected genes listed above using RNA extracted from whole seedlings. Upon recovery, none of genes exhibited a significant induction (*i.e.*, below a 2-fold change induction), when compared to the non-treated control (Figure 6B). Similar results were observed when using RNA extracted from roots (Figure S6B). The reversibility in expression is consistent with the idea that the induction of these genes relates to hyperosmotic stress. In order to correlate changes of gene expression upon recovery to changes in nuclear morphology, we also analysed nuclear shape upon release of hyperosmotic stress. After a 0.3 M mannitol treatment, root meristematic nuclei exhibited a deformed shape as previously shown, when compared to non-treated plants (Figures 7A and 7B). While nuclear shape remained unchanged after the additional 7 hours in the control medium (Figure 7C), the deformed nuclei observed in treated plants retrieved their original shape upon their transfer to control medium for 7 hours (Figure 7D). No statistical differences in nuclear circularity and

area could be detected between treated and untreated plants upon recovery ($n_{control}$ = 70, $n_{treated}$ = 61, *p*-values 0.74 and 0.56, respectively; Figures 7E and 7F).

Nuclear stiffening upon hyperosmotic stress is reversible

To link these changes to mechanical properties of the nucleus we performed measurements of nuclear stiffness on WT meristematic nuclei after mannitol treatment and upon recovery. Using both micro-rheometry and AFM, we found that mannitol-treated nuclei indeed become softer when the osmolarity of the medium is decreased. In the end, mannitol-treated-then-rescued nuclei exhibited an apparent elastic modulus that was comparable to that of the untreated iso-osmotic control (in AFM *p*-values control vs. recovery = 0.46; in micro-rheometry *p*-values control vs. recovery = 0.778; Figures 7G and 7H).

Interestingly, DAPI staining of the nuclei under micro-rheometry measurements revealed changes in the organization of the bright DAPI stained chromocenters associated with pericentromeric heterochromatin located at the nuclear periphery [45]. While in control and recovery nuclei (Figures S7A and S7D), the chromocenters were scattered as bright DAPI signals at the nuclear periphery, they appeared more clustered in the mannitol treated nucleus (Figure S7C). Conversely, when we treated the seedlings with hypo-osmotic stress (16h-water incubation), the chromocenters were more diffuse in isolated nuclei, while the size of the nuclei was increasing ($n_{control}$ n = 45, $n_{treated}$ = 32 , *p*-value = 9.06e-8, Figures S7B and S7H). Such nuclei seemed very soft and fragile. However we could not quantitatively assess this trend: only very few nuclei could be handled for micro-rheometry measurements (n = 5) providing no statistically significant bias (*p*-value = 0.265, Figure 7 H). We believe that we could only measure the stiffer nuclei, since the softer ones were probably, in essence, too weak mechanically to be micro-manipulated. Consistent with this hypothesis, the nuclei that we could mechanically test were indeed significantly smaller (mean area 27.6 ± 8 μm^2) than those that we could not handle (n=8, mean area 63.4 ± 10 μm^2, with a *p*-value of 0.047).
The discrepancy in DAPI staining was also observed at the tissue level, when analyzing nuclei in the root tips of WT, mannitol or water-treated seedlings (Figure S7E-S7G). However, we could not detect a significant increase of the nuclear area in root meristems of seedlings treated with water compared to control plants ($n_{control}$ = 164, $n_{treated}$ = 174 , *p*-value = 0.4, Figure S7I). In addition there was no clear changes in circularity (*p*-value = 0.12 Figure S7J), suggesting that the multicellular environment may prevent such hypo-osmotic environment to exist *in vivo*. Yet, except for *HSPRO2*, in such hypo-osmotic conditions, we

could observe a strong decrease in the transcript level of touch-induced genes when compared to WT control, between1.47- and 333-fold change (Figure S7M). However the response was very limited in *gip1gip2* with a fold change between 1.14 and 3.84 (Figure S7N) and no further nuclear deformation was observed as well (Figures S7 K-S7L).

Altogether, the reversibility of the nucleus response to hyperosmotic stress further supports a scenario in which nuclear shape and stiffness homeostasis is under control, linked to transcriptional program, and for which, the GIP proteins play a major, negative, regulatory role. Conversely, the nuclear response to hypo-osmotic stress leads to nuclear expansion on isolated nuclei and negative regulation of the touch gene expression *in planta* (Figure 7I).

Discussion

We show a reduction of both nuclear area (by 20%) and circularity (by 9%), an increase in nuclear stiffness (by a factor of 3 to 10) as well as a significant induction of touch response genes occur in a narrow window of hyperosmotic conditions (above 0.3 M and below 0.4 M mannitol). Importantly, these responses are reversible in iso-osmotic conditions, suggesting a mechanical response of the nucleus which may involve GIP/MZT1 proteins since *gip1gip2* mimic all the observed responses in a constitutive way. Because the *gip1gip2* nuclei are constitutively stiff, we propose that their increased resistance to hyperosmotic stress is in part provided by mechanical shielding through nuclear stiffening (Figure 7I).

Nuclear shape and stiffness may easily be related : nucleoplasm crowding following hyperosmotic stress may reduce nucleus size and increase its density, and thus its stiffness. Yet, the observation that a similar phenotype exists in the *gip1gip2* mutant suggests that this response is not passive, but actively regulated by nuclear envelope components, likely through the global spatial reorganization of chromatin. These data in a tissue context echo the role of nuclear mechanics in single cells in animals. Indeed, nuclear mechanical structure is essential to drive nuclear shape and transcriptional gene regulation [46]. For instance, nucleus stiffness positively scales with matrix stiffness, and this response involves lamins A and is accompanied by transcriptional changes [47]. Although maintenance of nuclear shape depends, in part at least on the nucleoskeleton and chromatin [18,48], these components do not have overlapping roles : lamin A would provide a robust enough structure to resist large nuclear deformation, while chromatin would govern nuclear stiffness in smaller deformations [49]. Of note, in line with our results, nuclear deformations in response to a hyperosmotic stress were also observed in isolated chondrocytes and were accompanied by chromatin condensation in specific regions within the nucleus [3]. More recently, NaCl-induced

hyperosmotic stress was shown to disrupt chromatin organization, with associated transcriptional changes as well [50]. The exact relationship between hyperosmotic stress and gene expression remains to be fully characterized in plants. Our analysis introduces the contribution of nuclear shape, stiffness and nuclear envelope factors in this network.

This work also raises new questions: how could the nuclear envelope control the nuclear response to osmotic conditions? As nuclear pores are too permissive to allow a pressure build-up inside the nucleus, this may likely involve the chromatin itself. This proposition is consistent with the reported impaired centromeric chromatin organization in the *gip1gip2* [37]. Thus, GIP would indirectly control the gel-like properties of chromatin in response to osmotic conditions. Chromatin remodeling can also make nuclei more compact in animal cells [51], and chromatin can become more compact upon hyperosmotic treatment in plants [52] . Therefore, our proposition may also be applicable beyond the plant kingdom. As we also found that a mutant better resists hyperosmotic stress than the WT, our work not only integrates nuclear mechanics in the plant response to drought, it may also open the way for a better understanding of how plants cope with water stress.

Acknowledgments

This work was supported by the Centre National de la Recherche Scientifique (CNRS, defi Mecanobio, NEstress 2016-2018), by Fondation Schlumberger pour l'Education et la Recherche (FSER 2016-2018), by the European Research Council Grants ERC-2013-CoG-615739 "MechanoDevo", by the IdEX international PhD program (unista, Strasbourg) and by HFSP Grant 2018, RGP, 009. This study was partially supported by the labex «Who AM I ?», labex ANR-11-LABX- 0071 and the Université de Paris, Idex ANR-18-IDEX-0001 funded by the French Government through its «investments for the future» program. We acknowledge discussions with members of the COST Action CA1612 INDEPTH network. We thank J. Fuchs (IPK, Gatersleben) for providing us flow cytometry sorting of nuclei as well as S. Koechler and A.Alioua at IBMP Gene Expression Analysis platform. We are grateful to K. Graumann for providing fluorescent-tagged SUN1 lines, as well as to Elise Hoffmann, L. Barret, and P. Johann to Berens for their technical help. We thank Jean-Pierre Henry for fruitful discussions about nuclear pores and mechanical regulation.

Author contributions

Conceptualization, A.A, M.E.C and O.H; Methodology, A.A, J.M., M.E.C, O.H, P.M.; Investigation, A.A., G.H., M.E.C., P.M., R.G.; Writing-original draft, M.E.C, O.H. and R.G.,

Writing-review & editing, A.A , M.E.C, O.H., P.M., R.G. and S.G. ; Funding acquisition, A.A., M.E.C., and O.H.; Visualization A.A., P.M., R.G. and S.G.; Resources, M.E.C.; Supervision, M.E.C. and O.H.

Declaration of interests

The authors declare no competing interests.

Figure Legends

Figure 1. **Nuclear shape is altered in the presence of hyperosmotic stress in WT *Arabidopsis* root tips.**

(A-B) Analysis of the nuclear shape in root tips by confocal microscopy of 9-day-old seedlings expressing SUN1-GFP in absence (A) or presence (B) of a 16h-long treatment with 0.3 M mannitol (Z max, optical sections of 0.7 µm). Representative images are presented. Scale bars are 5 µm.

(C-F) Quantification of various nuclear parameters were evaluated in 2D and 3D dimensions. Measurements were performed in the region delineated by the white frame in (A-B). In 2D, nuclear circularity (C) and nuclear area (E) were evaluated on control (n = 99) and treated (n = 98) plants. The *p*-values after Student's t-test are 3.23e-16 and 2.12e-11, indicating significant differences between the data, $p < 0.001$ (***). In 3D, nuclear sphericity (D) and volume (F) were evaluated on control and treated plants (n = 20). The *p*-values after Student's t-test are 0.0006 and 0.00012, respectively, indicating significant differences between the data $p < 0.001$ (***).

(G-H) Cell volume (G) and nuclear/cell volume ratio (F) were also evaluated on the same samples used for 3D measurements. The *p*-values after Student's t-test are 0.193 and 0.0001, indicating non-significant differences in changes in cell volume between control and treated samples but a significant change in nuclear/cell volume ($p < 0.001$, ***) related to main change of nuclear volume in response to hyperosmotic stress. See also Figure S1.

Figure 2: Nuclear shape defects are stable in the *gip1gip2 Arabidopsis* root tip upon hyperosmotic stress.

(A) Graphical representation (not to scale) of the localization of GIP protein in normal WT conditions and *gip1gip2* knocked down phenotype at the cellular level.

(B-C) Analysis of the nuclear shape in root tips by confocal microscopy (Z max, optical sections of 0.7 µm) in 9-day-old *gip1gip2* seedlings expressing SUN1-GFP in absence (B, n = 74) or presence (C, n = 45) of a 16h-long treatment with 0.3 M mannitol. Scale bars are 5 µm. (D-E) Quantification of nuclear parameters, circularity (D) and nucleus area (E) were evaluated on control and treated plants. The *p*-values after Student's t-test are 0.11 and 0.87, respectively indicating no significant differences between the data (n.s.). Measurements were performed in the region delineated by the white frame in (B-C). See also Figure S2.

Figure 3. Resistance of *gip1gip2* root tip cells to severe hyperosmotic conditions and analyses of nuclear shape and plant growth changes.

(A-B) Confocal analysis of root meristems of 9-day-old Arabidopsis expressing SUN1-GFP in presence of 0.4 M (A) and 0.6 M (B) mannitol stress (16h treatment) in WT seedlings (n = 8; n = 5; respectively) and mild *gip1gip2* (n = 10). Dead cells were revealed upon propidium iodide staining (magenta). Scale bars are 5 µm.

(C-D) Quantification of nuclear parameters, the circularity (C) and the area (D) of the nuclei were evaluated in WT in both mannitol treatments compared to control ($n_{control} = 38$, $n_{0.4\ M} = 39$ and $n_{0.6\ M} = 41$). Between control/0.4 M and control/0.6 M *p*-values (Student's t-test) are 2.903e-9, 1.515e-6 and 1.604e-10, 3.581e-10 respectively for each parameters indicating a significant change between control and severe hyperosmotic conditions ($p < 0.001$, ***). No significant change (n.s.) was observed between nuclear parameters at 0.4 M and 0.6 M mannitol with *p*-values of 0.094 for nuclear circularity and 0.075 for nuclear area.

(E-F) Quantification of nuclear circularity (E) and area (F) of the nuclei in mild *gip1gip2* in both mannitol treatments compared to control ($n_{control} = 57$, $n_{0.4\ M} = 22$, $n_{0.6\ M} = 43$). Using Student's t-test no significant changes (n.s.) were observed between control/0.4 M or control/0.6 M with *p*-values of 0.329, 0.614 and 0.989, 0.534 for nuclear circularity and area, respectively, nor between 0.4 M and 0.6 M conditions with *p*-values of 0.195 and 0.617, respectively.

(G-I) Mild *gip1gip2* phenotype compared to WT using 9-day-old seedlings transferred for 2 days on 0.4 M and 0.6 M mannitol as well as on control media. Main root growth was evaluated through the measurement of root length on growth control conditions ($n_{WT} = 12$, $n_{gip1gip2} = 10$), 0.4 M mannitol ($n_{WT} = 13$, $n_{gip1gip2} = 10$) and 0.6 M mannitol ($n_{WT} = 12$; $n_{gip1gip2} = 13$). Using Mann Whitney test, different letters above the error bars indicate significant differences at $p < 0.01$. Three individual experiments were repeated. (H-I) Senescence in leaves of WT and *gip1gip2* maintained on 0.4 M and 0.6 M mannitol for 15

days. Representative images are presented, on each figure, the left panel presents magnification of WT and *gip1gip2* leaf rosettes, respectively. Scale bars are 0.2 cm.

(J-L) Mild and strong *gip1gip2* phenotypes compared to WT using 9 day-old seedlings transferred to 0.3 M mannitol for 5 days. Every day, main root length was measured on control media :WT (n = 6), mild *gip1gip2* (n = 7) and strong *gip1gip2* (n = 6) and on 0.3 M mannitol :WT (n = 7), mild *gip1gip2* (n = 6) and strong *gip1gip2* (n = 7). Comparing mean values between control and treated samples using Mann Whitney test, no significant differences were found for mild and strong *gip1gip2* phenotypes with *p*-values of 0.095 and 0.63, respectively while a *p*-value of 0.031 was found for WT ($p < 0.05$, *). Three individual experiments were repeated. See also Figure S3.

Figure 4: Hyperosmotic stress and *gip1gip2* mutations stiffen the nuclei.

(A-D) Micro-rheometry on isolated nuclei. (A) An isolated nucleus (see, dashed red circle) is trapped between microplates, one rigid, the other flexible with calibrated stiffness using micro-rheometry measurement. The uniaxial nucleus deformation is under controlled applied forces. Fluorescence imaging of an isolated WT SUN1-GFP nucleus (green) stained with DAPI (left). Bright field imaging of the nucleus before (center) and after (right) compression between the two microplates: deformation occurred reflecting its low stiffness. (B) Fluorescence imaging of a *gip1gip2* SUN1-GFP nucleus trapped (left) and compressed (right) in the micro-rheometer: almost no deformation occurred reflecting its high stiffness. Scale bars are 5 µm. (C) Principle of the micro-rheometry to measure nuclear stiffness. The force applied to the nucleus is F = kd, where d is the deflection of the flexible microplate of spring constant k. The elastic modulus was obtained by dividing the force F by the apparent contact area and relative nuclear shortening between the plates, *i.e.* nuclear strain. Comparison of the elastic moduli (kPa) between *gip1gip2* (n = 17) and WT SUN1-GFP nuclei treated (n = 11) or not (n = 17) with 0.3 M mannitol, *p*-values from Mann-Whitney tests are WT/ WT treated: 0.0029 (significant $p < 0.01$); WT/*gip1gip2*: 0.000107 (significant $p < 0.001$); and WT treated/*gip1gip2* : 0.643 (n.s.).

(E-J) AFM analysis of nuclei from root meristems. (E) Principle of the AFM to measure nuclear stiffness. (F-H) The AFM tip was positioned on a nucleus (GFP signal) isolated from root squashing after cell wall digestion of WT (F) and *gip1gip2* (H) and the acquisition of a matrix of force curves (100 curves) was acquired for WT (G) and *gip1gip2* nuclei (H, right inset).

(G-I) Topography was obtained in WT (G) and mutant (I) with the PeakForce ® QNM (Quantitative Nanomechanical Mapping). Scale bars are 5 µm. (J) Comparison of the elastic

moduli between WT (n = 14 nuclei in 3 independent roots) and *gip1gip2* nuclei (n = 13 nuclei in 3 independent roots) *p*-values from Mann-Whitney test are 0.00288 (significant $p < 0.01$). See also Figure S4 and Video S1 and S2.

Figure 5: Transcriptomic analysis of *gip1gip2* compared to WT.

(A) Vein diagram shows the overlap between up-regulated genes in *gip1gip2* and the touch response in WT (Lee et al., 2005). R factor and *p*-value are indicated using the hypergeometric test.

(B) Relative transcript levels of 18 touch-induced genes (Figure S5E) in *gip1gip2* compared to WT. RT qPCR were performed on RNA isolated from 9-day-old seedlings using specific primers, with 3 technical replicates and 3 biological replicates. SDs are indicated. See also Figure S5, Tables S1 and S2.

Figure 6. Relative mRNA level in response to hyperosmotic stress.

(A-B) Analysis of the relative mRNA levels of selected touch-induced genes in 9-day-old seedlings in presence of 0.3 M mannitol during 16h and after 7h of recovery (B) on normal growth medium compared to control (no treatment). RT qPCR were performed using RNA extracted from 9-day-old seedlings and specific primers, with 3 technical replicates and 3 biological replicates. SDs are indicated. See also Figure S6 and Table S2.

Figure 7. Changes of nuclear shape and elastic modulus are reversible upon hyperosmotic stress.

(A-B) Representative images of nuclei in root meristems. Nine-day-old WT SUN1-GFP seedlings from control and treated seedlings with 0.3 M mannitol for 16h are presented.

(C-D) Representative images of nuclei in root meristems of control (C) and mannitol-treated seedlings (D) upon recovery on normal growth medium for 7 hours. Scale bars are 5 µm.

(E-F) Quantification of nuclear parameters, circularity (E) and nuclear area (F) upon recovery on control and treated plants. The *p*-values after Student's t test are 0.73 and 0.56, respectively, indicating no significant changes between untreated and recovering samples (n.s.). Measurements were performed in the region delineated by the white frame in (C, D).

(G-H) Evaluation of elastic modulus using AFM (G) on nuclei from squashed and lysed root meristem of seedlings treated with mannitol (n = 10) and upon recovery (n = 10) of a mannitol treatment compared to control (n = 7). Using Mann Whitney test *p*-values were : 0.027 between control and mannitol (*); 0.0004 between mannitol and recovery (**); 0.46 (n.s.) between control and recovery. Evaluation of elastic modulus using micro-rheometry on

isolated nuclei from seedlings treated with mannitol (n = 11) and upon recovery (n = 8) compared to control (n = 7) or seedlings treated with water (n = 5). Using Mann Whitney test, *p*-values were : 0.005 between control and mannitol(**); 0.0045 between mannitol and recovery (**); 0.778 (n.s.) between control and recovery; 0.265 (n.s.) between control and water. (I) Graphical abstract: Changes in nuclear shape and mechanics related to osmotic stress and touch gene expression. Implication of GIPs in plant growth sensitivity to hyperosmotic stress. See also Figure S7.

STAR METHODS

CONTACT FOR REAGENT AND RESOURCE SHARING

All plant lines are available for sharing. Further information for resources and reagents should be forwarded and attended by the Lead Contact, Marie-Edith Chabouté (marie-edith.chaboute@ibmp-cnrs.unistra.fr).

EXPERIMENTAL MODEL AND SUBJECT DETAILS

Plants

Wild type *pSUN1::SUN1-GFP* and *gip1gip2* SUN1-GFP lines were described previously [34,38]. The *gip1gip2* mutant [36] was investigated for transcriptomic analyses, using 2 types of phenotypes *i.e.* T12 (mild phenotype) and T34 (strong phenotype), as described in Figure S2. WT background of *gip1gip2*, *i.e.* Ws x Col-0, was used as a control. Seedlings were grown *in vitro* on 1/2 Murashige and Skoog (MS) medium (SERVA Electrophoresis) in presence of 1% sucrose and 1.2% agar at 20 °C under long day conditions (16-h light 70µmol/m2 per second of fluorescent lighting/8-h dark).

METHOD DETAILS

Osmotic stress conditions for nuclear properties analyses

For osmotic treatments, sterilized seeds were germinated on ½ MS medium and 9-day-old seedlings, were transferred in ½ MS liquid medium containing 0.3 M mannitol for 16h (hyperosmotic stress) or water (hypoosmotic stress). As a control, seedlings were transferred to ½ MS liquid medium.

Plant growth analysis under hyperosmotic stress conditions

Seedlings were grown for 9 days on ½ MS medium and then transferred to medium containing 0.3 M, 0.4 M and 0.6 M mannitol. Pictures of plates were taken before and after treatment either every day after treatment (0.3 M mannitol) or after 2 days of treatment (0.4 and 0.6 M mannitol). Root growth was evaluated using the segmented line measure tool plugin in ImajeJ using a line traced between 2 points.

Propidium iodide and DAPI staining on whole mount roots

Root meristem of 9-old seedlings were observed under confocal microscopy using 2µg/mL propidium iodide (Sigma Aldrich) which reveal cell wall in viable cells and enter into the cell when cell is dead. Chromatin staining was performed on SUN1-GFP seedlings by incubating the roots in FACS buffer containing DAPI (2µg/mL) for 10 min and roots were observed afterwards.

Nuclei preparation for micro-rheometry analysis

Nuclei were prepared by chopping root tips from 9-day-old seedlings in a Petri dish with a razor blade in 400 µl of ice-cold commercial nuclei isolation buffer containing DAPI (Cystein UV precise P, Sysmex Partec, Germany) and samples were filtered through a 30 µm mesh filters to remove debris. Nuclei were then concentrated in a pellet after a 5 min centrifugation 3000 rpm at 4°C. Pellet was either resuspended in culture medium with or without mannitol and kept on ice before micro-rheometry measurements.

Micro-rheometry measurement of nuclear stiffness

The experimental chamber was filled with medium containing nuclei. Isolated nucleus was captured between two parallel microplates, one rigid, the other flexible with a calibrated stiffness k. The force applied on the nucleus upon compression was given by F= k d, were d is the flexible plate deflection. All measurements were carried out with a flexible plate of spring constant k= 3.1 mN/m. The contact areas between the plates and the nucleus were estimated by assuming a circular contact. The apparent contact diameters D_F and D_R (respectively for the flexible and rigid plate) where then measured on bright field images. Then the stress σ applied on the nucleus was defined as F/A, where A is the contact area, with $A= \pi D^2$. However, since D_F and D_R was usually not exactly the same, leading to two different stress values on the flexible and rigid plate, we retained their mean value $\sigma = 2F/\pi\ [1/D_F^2+1/D_R^2]$. The uniaxial nucleus strain perpendicular to plates was defined as $\varepsilon = (L-L_0)/L_0$, where L_0 and L are respectively the nucleus length (distance between the parallel microplates) before and

after compression. The nucleus was submitted to increasing compression steps, and the values of ε and σ were reported for each step. Stress-strain data σ(ε) were then fitted by a linear relationship the slope of which was retained as the value of the apparent elastic modulus E of the nucleus. The static apparent elastic modulus of the nucleus is then given by E= σ/ε.

AFM – material and analyses

Roots from 9-day old seedlings were put on poly L-lysin plates and cell wall was digested in 100 µl of digestion mix (2.5 % pectinase, 2.5 % cellulase, 2.5 pectolyase in MTBS buffer as previously described [37]. Then root tip was squashed and covered by MTBS buffer to isolate the nuclei (50 mM Pipes, 5 mM EGTA, and 5 mM MgSO4, pH 6.9 in presence of 0.1% Triton X-100). Atomic force microscopy was performed using Bioscope catalyst (Bruker) which was coupled with an optical epifluorescence macroscope (MacroFluo-Leica) equipped with a long distance Mitutoyo 10x air objective lens. The PeakForce ® QNM (Quantitative Nanomechanical Mapping) mode was used for this study. The selected AFM cantilever had a theoretical spring constant of 0.4N/m and the pyramidal tip had a theoretical curvature radius <40nm. Before each experiment, the deflection sensitivity of the cantilever was calibrated on Sapphire and its spring constant was also calibrated by thermal tuning. A matrix of force curves was acquired using the following parameters: Images: 100 μm^2, 128px^2, PeakForce setpoint = 1-5nN, Force curves: Ramp size = 2-5 µm, applied force = 8-10nN. The quantifications of the elastic modulus based on raw force curves were achieved with the processing software Nanoscope Analysis (Bruker). Briefly, the quantification of the apparent elastic modulus (Ea) was extracted via the application of a theoretical model (Sneddon) for an indentation I < 100 nm. The measured elastic modulus reflected the stiffness of the nucleus. Each curve was analysed individually.

RNA extraction and sequencing

Total RNA was extracted from 9-day-old seedlings using Nucleospin RNA Plant kit (Macherey-Nagel, Düren, Germany) according to manufacturer's instructions. For each preparation around 30 mg of frozen plant material was ground in extraction buffer in a Precelly 24 crusher (Bertin Technologie, Montigny-les-Bretonneux, France) for 2 x 30 s at 3600 rpm in presence of 0,75/1,0 mm glass beads. Purified RNAs were resuspended in 40 µl water. Quantity and quality of the extracted RNAs were determined using QuBit RNA HS assay kit (Thermo Fisher Scientific, Waltham, USA) and a Bioanalyser 2100 (Agilent Technologies, Santa Clara, USA), respectively. RNA Seq was done by Fasteris SA (Plan-les-

Ouates, Switzerland) on samples of 2 µg of RNA in 20 µl. The sequencing was performed on Illumina in 125bp on single end mode.

Transcriptomic data analysis

Raw reads were quality checked with FastQC (v0.10.1) and cleaned with cutadapt (v1.8.1). Mapping was performed against the *Arabidopsis thaliana* reference genome (from Araport11) using Hisat2 (v2.1.0) and the read counting was done using FeatureCounts (v1.6.2). Differential expression analysis and corresponding graphs were done using the DESeq2 package (v1.22.2). Finally the GO analysis was done with the latest version of the DAVID online tool.

RNA extraction and Real-Time RT-qPCR

Either whole 9-day-old seedlings or root tips from 9-day-old seedling were collected and snap-frozen in liquid nitrogen. For each experiment at least 3 independent biological replicates were used. Total RNA was extracted followig kit 'NucleoSpin® RNA Plant, Macherey-Nagel' protocol (Macherey-Nagel, Düren, Germany). For qRT-PCR, 2.5 µg of RNA was used to synthesize cDNA using random hexamer primers (IDT) and the protocol "SuperScript® IV (SSIV) First-strand and cDNA Synthesis Reaction" (Invitrogen). qRT-PCR was performed on Light Cycler thermocycler 480 II (Roche) with SYBR Green Master Mix (Bio-Rad). Primers used are described in in SI Table S1. The cDNA quantification was made with the ΔΔCt method, which considers the amplification efficiency ([1+E]- ΔΔCt) and normalized to ACTIN2 [53].

Confocal Microscopy

Confocal images were recorded with a Zeiss LSM 700 microscope equipped with 20×/0.8 NA lens. The excitation and emission wavelengths for the fluorescent protein GFP are 488 nm and 510 nm, respectively. For propidium iodide observations, the excitation and emission wavelengths were 555 nm and 617 nm, respectively. Images were captured using Z stacks with 0.7 µm Z slice intervals. For DAPI observations, the excitation and emission wavelengths were 405 nm and 500 nm. Observations were performed in multi-tracking mode using 405-, 488-, or 555-nm laser excitation.

QUANTIFICATION AND STATISTICAL ANALYSIS

Nuclear parameters measurements

The confocal images were analysed using ImageJ. The nuclear circularity was measured using a Plugin NucSeg in ImajeJ developed by J. Mutterer (IBMP). The plugin gives a detailed analysis of several parameter of the nucleus including circularity with the formula, *i.e.* Circularity = $4\pi \times$ area/ perimeter^2. A circularity of 1 corresponds to a perfect circle. Nuclear volume and sphericity were evaluated using 3D manager and segmentation editor in Fiji (ImageJ). The volume of the 3D object is evaluated in calibrated unit, *i. e.* the number of voxels multiplied by the calibrated volume of one voxel. Compactness (sphericity) is the normalized ratio between the surface and the volume, it should be close to value 1 for a perfect sphere. Measurements were performed in the epidermal and cortex layers of the root, *i.e.* in the tissues directly exposed to mannitol.

Statistical tests

The distribution of the data was evaluated using Shapiro-Wilk test to determine if they follow a normal law. Accordingly, we used either two tailed Student-t-test or Mann-Whitney test. The Student t-test was performed to study the significance of the difference between two populations for nuclear circularity and area data. The variances of the population in all the sets of data were tested using F-test. For low data number, Mann-Whitney test was used. Sample size and statistical tests are indicated in the figure captions.

DATA AND CODE AVAILABILITY

This work does not involve the production of large datasets and uses published plugins or image analysis tools.

Video S1: **Nuclear deformation of a WT nucleus using micro-rheometry** In our experimental conditions, nucleus was kept in control medium. A bright field microscopy imaging is presented. The rigid (bottom) plate is moved up thus compressing the nucleus against the flexible (top) plate which is deflected up like a regular spring.

Video S2: **Nuclear deformation of a treated WT nucleus using micro-rheometry.** In our experimental conditions, nucleus was kept in 0.3 M mannitol medium. A bright field microscopy imaging is presented.

References

1. D'Arcy Thompson, W. (1917). On Growh and Form (Cambridge, UK: Cambridge

University Press).

2. Discher, D.E., Janmey, P., and Wang, Y.L. (2005). Tissue cells feel and respond to the stiffness of their substrate. Science. *310*, 1139–1143.
3. Irianto, J., Swift, J., Martins, R.P., McPhail, G.D., Knight, M.M., Discher, D.E., and Lee, D.A. (2013). Osmotic challenge drives rapid and reversible chromatin condensation in chondrocytes. Biophys J *104*, 759–769.
4. Lovett, D.B., Shekhar, N., Nickerson, J.A., Roux, K.J., and Lele, T.P. (2013). Modulation of Nuclear Shape by Substrate Rigidity. Cell Mol Bioeng *6*, 230–238.
5. Uhler, C., and Shivashankar, G. V (2017). Regulation of genome organization and gene expression by nuclear mechanotransduction. Nat. Rev. Mol. Cell Biol. *18*, 717–727.
6. Miroshnikova, Y.A., Nava, M.M., Wickström, S.A., and Wickstrom, S.A. (2017). Emerging roles of mechanical forces in chromatin regulation. J. Cell Sci. *130*, 2243–2250.
7. Cho, S., Irianto, J., and Discher, D.E. (2017). Mechanosensing by the nucleus: From pathways to scaling relationships. J Cell Biol *216*, 305–315.
8. Maharana, S., Iyer, V.K., Jain, N., Nagarajan, M., Wang, Y., and Shivashankar, G. V (2016). Chromosome intermingling—the physical basis of chromosome organization in differentiated cells. Nucleic Acids Res. *44*, 5148–5160.
9. Dupont, S., Morsut, L., Aragona, M., Enzo, E., Giulitti, S., Cordenonsi, M., Zanconato, F., Le Digabel, J., Forcato, M., Bicciato, S., *et al.* (2011). Role of YAP/TAZ in mechanotransduction. Nature *474*, 179–183.
10. Alam, S.G., Zhang, Q., Prasad, N., Li, Y., Chamala, S., Kuchibhotla, R., Kc, B., Aggarwal, V., Shrestha, S., Jones, A.L., *et al.* (2016). The mammalian LINC complex regulates genome transcriptional responses to substrate rigidity. Sci. Rep. *6*, 38063.
11. Mammoto, A., Mammoto, T., and Ingber, D.E. (2012). Mechanosensitive mechanisms in transcriptional regulation. J Cell Sci *125*, 3061–3073.
12. Poh, Y.C., Shevtsov, S.P., Chowdhury, F., Wu, D.C., Na, S., Dundr, M., and Wang, N. (2012). Dynamic force-induced direct dissociation of protein complexes in a nuclear body in living cells. Nat Commun *3*, 866.
13. Tajik, A., Zhang, Y., Wei, F., Sun, J., Jia, Q., Zhou, W., Singh, R., Khanna, N., Belmont, A.S., and Wang, N. (2016). Transcription upregulation via force-induced direct stretching of chromatin. Nat Mater *15*, 1287–1296.
14. Hampoelz, B., Azou-Gros, Y., Fabre, R., Markova, O., Puech, P.H., and Lecuit, T. (2011). Microtubule-induced nuclear envelope fluctuations control chromatin dynamics in Drosophila embryos. Development *138*, 3377–3386.

15. Elosegui-Artola, A., Andreu, I., Beedle, A.E.M., Lezamiz, A., Uroz, M., Kosmalska, A.J., Oria, R., Kechagia, J.Z., Rico-Lastres, P., Le Roux, A.L., *et al.* (2017). Force Triggers YAP Nuclear Entry by Regulating Transport across Nuclear Pores. Cell *171*, 1397-1410 e14.
16. Kirby, T.J., and Lammerding, J. (2018). Emerging views of the nucleus as a cellular mechanosensor. Nat Cell Biol *20*, 373–381.
17. Stephens, A.D., Liu, P.Z., Kandula, V., Chen, H., Almassalha, L.M., Herman, C., Backman, V., O'Halloran, T., Adam, S.A., Goldman, R.D., *et al.* (2019). Physicochemical mechanotransduction alters nuclear shape and mechanics via heterochromatin formation. Mol. Biol. Cell. *17*:2320-2330.
18. Alisafaei, F., Jokhun, D.S., Shivashankar, G. V, and Shenoy, V.B. (2019). Regulation of nuclear architecture, mechanics, and nucleocytoplasmic shuttling of epigenetic factors by cell geometric constraints. Proc Natl Acad Sci U S A *16*, 13200–13209.
19. Durand-Smet, P., Gauquelin, E., Chastrette, N., Boudaoud, A., and Asnacios, A. (2017). Estimation of turgor pressure through comparison between single plant cell and pressurized shell mechanics. Phys Biol *14*, 55002.
20. Asnacios, A., and Hamant, O. (2012). The mechanics behind cell polarity. Trends Cell Biol. *22*, 584-591.
21. Finan, J.D., and Guilak, F. (2010). The effects of osmotic stress on the structure and function of the cell nucleus. J Cell Biochem *109*, 460–467.
22. Xiong, L., Schumaker, K.S., and Zhu, J.K. (2002). Cell signaling during cold, drought, and salt stress. Plant Cell *14 Suppl*, S165-83.
23. Kim, J.M., Sasaki, T., Ueda, M., Sako, K., and Seki, M. (2015). Chromatin changes in response to drought, salinity, heat, and cold stresses in plants. Front Plant Sci *6*, 114.
24. Kreps, J.A., Wu, Y., Chang, H.S., Zhu, T., Wang, X., and Harper, J.F. (2002). Transcriptome changes for Arabidopsis in response to salt, osmotic, and cold stress. Plant Physiol *130*, 2129–2141.
25. Zeller, G., Henz, S.R., Widmer, C.K., Sachsenberg, T., Ratsch, G., Weigel, D., and Laubinger, S. (2009). Stress-induced changes in the Arabidopsis thaliana transcriptome analyzed using whole-genome tiling arrays. Plant J *58*, 1068–1082.
26. Lee, D., Polisensky, D.H., and Braam, J. (2005). Genome-wide identification of touch- and darkness-regulated Arabidopsis genes: a focus on calmodulin-like and XTH genes. New Phytol *165*, 429–444.
27. Braam, J. (2005). In touch: plant responses to mechanical stimuli. New Phytol. *165*, 373–389.

28. Coutand, C., Chevolot, M., Lacointe, A., Rowe, N., and Scotti, I. (2010). Mechanosensing of stem bending and its interspecific variability in five neotropical rainforest species. Ann Bot *105*, 341–347.
29. Landrein, B., Kiss, A., Sassi, M., Chauvet, A., Das, P., Cortizo, M., Laufs, P., Takeda, S., Aida, M., Traas, J., *et al.* (2015). Mechanical stress contributes to the expression of the STM homeobox gene in Arabidopsis shoot meristems. Elife *4*, e07811.
30. Goto, C., Tamura, K., Fukao, Y., Shimada, T., and Hara-Nishimura, I. (2014). The Novel Nuclear Envelope Protein KAKU4 Modulates Nuclear Morphology in Arabidopsis. Plant Cell *26*, 2143–2155.
31. Pawar, V., Poulet, A., Detourne, G., Tatout, C., Vanrobays, E., Evans, D.E., and Graumann, K. (2016). A novel family of plant nuclear envelope-associated proteins. J Exp Bot *67*, 5699–5710.
32. Wang, H., Dittmer, T.A., and Richards, E.J. (2013). Arabidopsis CROWDED NUCLEI (CRWN) proteins are required for nuclear size control and heterochromatin organization. BMC Plant Biol. *13*, 200.
33. Dittmer, T.A., Stacey, N.J., Sugimoto-Shirasu, K., and Richards, E.J. (2007). LITTLE NUCLEI Genes Affecting Nuclear Morphology in Arabidopsis thaliana. Plant Cell *19*, 2793–2803.
34. Batzenschlager, M., Masoud, K., Janski, N., Houlne, G., Herzog, E., Evrard, J.L., Baumberger, N., Erhardt, M., Nomine, Y., Kieffer, B., *et al.* (2013). The GIP gamma-tubulin complex-associated proteins are involved in nuclear architecture in Arabidopsis thaliana. Front Plant Sci *4*, 480.
35. Janski, N., Herzog, E., and Schmit, A.C. (2008). Identification of a novel small Arabidopsis protein interacting with gamma-tubulin complex protein 3. Cell Biol Int *32*, 546–548.
36. Janski, N., Masoud, K., Batzenschlager, M., Herzog, E., Evrard, J.L., Houlne, G., Bourge, M., Chaboute, M.E., and Schmit, A.C. (2012). The GCP3-interacting proteins GIP1 and GIP2 are required for gamma-tubulin complex protein localization, spindle integrity, and chromosomal stability. Plant Cell *24*, 1171–1187.
37. Batzenschlager, M., Lermontova, I., Schubert, V., Fuchs, J., Berr, A., Koini, M.A., Houlne, G., Herzog, E., Rutten, T., Alioua, A., *et al.* (2015). Arabidopsis MZT1 homologs GIP1 and GIP2 are essential for centromere architecture. Proc Natl Acad Sci U S A *112*, 8656–8660.
38. Graumann, K., Runions, J., and Evans, D.E. (2010). Characterization of SUN-domain proteins at the higher plant nuclear envelope. Plant J *61*, 134–144.

39. Versaevel, M., Grevesse, T., and Gabriele, S. (2012). Spatial coordination between cell and nuclear shape within micropatterned endothelial cells. Nat. Commun. **3**, 671.
40. Desprat, N., Richert, A., Simeon, J., and Asnacios, A. (2005). Creep function of a single living cell. Biophys J *88*, 2224–2233.
41. Durand-Smet, P., Chastrette, N., Guiroy, A., Richert, A., Berne-Dedieu, A., Szecsi, J., Boudaoud, A., Frachisse, J.M., Bendahmane, M., Hamant, O., *et al.* (2014). A comparative mechanical analysis of plant and animal cells reveals convergence across kingdoms. Biophys J *107*, 2237–2244.
42. Sewelam, N., Oshima, Y., Mitsuda, N., and Ohme-Takagi, M. (2014). A step towards understanding plant responses to multiple environmental stresses: A genome-wide study. Plant, Cell Environ. 37, 2024-2035.
43. Gu, Y., Zebell, S.G., Liang, Z., Wang, S., Kang, B.H., and Dong, X. (2016). Nuclear Pore Permeabilization Is a Convergent Signaling Event in Effector-Triggered Immunity. Cell *166*, 1526-1538 e11.
44. Ghosh, R., Mishra, R.C., Choi, B., Kwon, Y.S., Bae, D.W., Park, S.-C.C., Jeong, M.-J.J., and Bae, H. (2016). Exposure to Sound Vibrations Lead to Transcriptomic, Proteomic and Hormonal Changes in Arabidopsis. Sci. Rep. *6*, 33370.
45. Fransz, P., De Jong, J.H., Lysak, M., Castiglione, M.R., and Schubert, I. (2002). Interphase chromosomes in Arabidopsis are organized as well defined chromocenters from which euchromatin loops emanate. Proc Natl Acad Sci U S A *99*, 14584–14589.
46. Isermann, P., and Lammerding, J. (2013). Nuclear mechanics and mechanotransduction in health and disease. Curr. Biol. *23*, 21.
47. Swift, J., Ivanovska, I.L., Buxboim, A., Harada, T., Dingal, P.C., Pinter, J., Pajerowski, J.D., Spinler, K.R., Shin, J.W., Tewari, M., *et al.* (2013). Nuclear lamin-A scales with tissue stiffness and enhances matrix-directed differentiation. Science *341*, 1240104.
48. Stephens, A.D., Banigan, E.J., and Marko, J.F. (2019). Chromatin's physical properties shape the nucleus and its functions. Curr Opin Cell Biol *58*, 76–84.
49. Stephens, A.D., Banigan, E.J., Adam, S.A., Goldman, R.D., and Marko, J.F. (2017). Chromatin and lamin A determine two different mechanical response regimes of the cell nucleus. Mol. Biol. Cell *28*, 1984–1996.
50. Amat, R., Bottcher, R., Le Dily, F., Vidal, E., Quilez, J., Cuartero, Y., Beato, M., de Nadal, E., and Posas, F. (2019). Rapid reversible changes in compartments and local chromatin organization revealed by hyperosmotic shock. Genome Res *29*, 18–28.
51. Heo, S.J., Thorpe, S.D., Driscoll, T.P., Duncan, R.L., Lee, D.A., and Mauck, R.L. (2015). Biophysical regulation of chromatin architecture instills a mechanical memory

in mesenchymal stem cells. Sci. Rep. 5, 16895.

52. Wang, Z., Casas-Mollano, J.A., Xu, J., Riethoven, J.-J.M., Zhang, C., and Cerutti, H. (2015). Osmotic stress induces phosphorylation of histone H3 at threonine 3 in pericentromeric regions of Arabidopsis thaliana. Proc. Natl. Acad. Sci. *112*, 8487–8492.

53. Livak, K.J., and Schmittgen, T.D. (2001). Analysis of Relative Gene Expression Data Using Real-Time Quantitative PCR and the 2−ΔΔCT Method. Methods *25*, 402–408.

54. Martin, M. (2011). Cutadapt removes adapter sequences from high-throughput sequencing reads. EMBnet.journal.

55. Cheng, C.Y., Krishnakumar, V., Chan, A.P., Thibaud-Nissen, F., Schobel, S., and Town, C.D. (2017). Araport11: a complete reannotation of the Arabidopsis thaliana reference genome. Plant J. *89*, 789-804

56. Huang, D.W., Sherman, B.T., and Lempicki, R.A. (2009a). Bioinformatics enrichment tools: Paths toward the comprehensive functional analysis of large gene lists. Nucleic Acids Res. 37, 1–13.

57. Huang, D.W., Sherman, B.T., and Lempicki, R.A. (2009b). Systematic and integrative analysis of large gene lists using DAVID bioinformatics resources. Nat. Protoc. *4*, 44–57.

58. Kim, D., Langmead, B., and Salzberg, S.L. (2015). HISAT: A fast spliced aligner with low memory requirements. Nat. Methods. *12*, 357–360.

59. Liao, Y., Smyth, G.K., and Shi, W. (2014). FeatureCounts: An efficient general purpose program for assigning sequence reads to genomic features. Bioinformatics. 30, 923–930

60. Love, M.I., Huber, W., and Anders, S. (2014). Moderated estimation of fold change and dispersion for RNA-seq data with DESeq2. Genome Biol. *15*, 550.

Key Resource Table

REAGENT or RESOURCE	SOURCE	IDENTIFIER
Chemicals, Peptides, and Recombinant Proteins		
D-Mannitol	Duchefa	Cat. No. M0803
Pectinase	Sigma	Product No. 17389
Cellulase	Yakult Pharmaceutical Industry Co., Ltd	https://www.yakult.co.jp/ypi/en/product/laboratory.html
Pectolyase Y-23	Duchefa	Product No. P8004.0001
PIPES	euromedex	REF 1124
Propidium iodide	SigmaAldrich	Product No.P4170
Cyber green	Roche	Cat. No. REF 04707516001
Critical Commercial Assays		
Nuclei extraction buffer : Cystein UV precise P,	Sysmex, Partec	Ref 05-5002
Nucleospin RNA Plant kit	Macherey-Nagel, Düren	Ref 740949.50
QuBit RNA HS assay kit	Thermo Fisher Scientific, Waltham, USA	Cat. No. Q32855
Bioanalyser 2100	Agilent Technologies, Santa Clara, USA	
Deposited Data		
GEO transcriptomic data	GSE133011	
Experimental Models: Organisms/Strains'		
Arabidopsis gip1gip2	[36]	Cross between *gip1* (GABI_213D01) and *gip2* (FLAG_36406)
Arabidopsis pSUN1::SUN1-GFP	[38]	
Arabidopsis gip1gip2 p35S::SUN1-YFP	[34]	Transformation of *gip1gip2* via floral dipping with *p35S::AtSUN1-YFP*
Arabidopsis : WT Col-0 x Ws	https://www-arabidopsis-org.insb.bib.cnrs.fr/servlets/TairObject?id=90&type=species_variant https://www.arabidopsis.org/servlets/TairObject?id=392&type=species_variant	Cross between WT Columbia-0 (NASC stock number: N1092) and WT Wassilewskija (NASC stock number: N2223)
Oligonucleotides		
Primers for qPCR, see table S2	This paper	N/A
Software and Algorithms		
ImageJ	https://imagej.net/Welcome	RRID:SCR_003070
Nugsec	https://github.com/mutterer/NucSeg	

Nanoscope Analysis	Bruker	
FastQC (v0.10.1)	N/A	https://www.bioinformatics.babraham.ac.uk/projects/fastqc/
The PeakForce ® QNM	Bruker	
cutadapt (v1.8.1).	[54]	https://cutadapt.readthedocs.io/en/stable/installation.html
Araport11	[55]	https://www.araport.org/
DESeq2 package (v1.22.2).	[56]	https://bioconductor.org/packages/release/bioc/html/DESeq2.html
Hisat2 (v2.1.0)	[57]	https://ccb.jhu.edu/software/hisat2/index.shtml
DAVID	[58,59]	https://david.ncifcrf.gov/
Zeiss LSM 700 microscope	https://www.zeiss.com/	N/A
FeatureCounts (v1.6.2).	[60]	https://doi.org/10.1093/bioinformatics/btt656

Figure 1

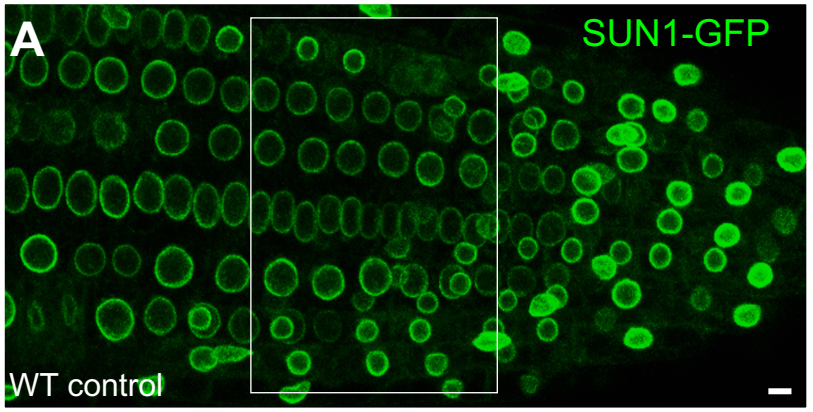
A
SUN1-GFP
WT control

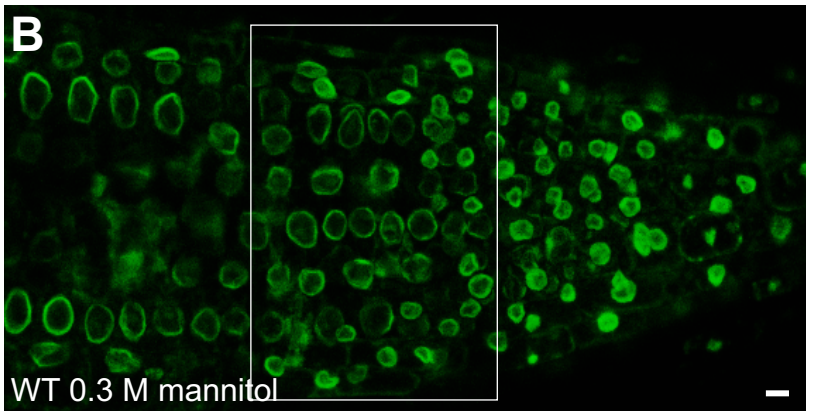
B
WT 0.3 M mannitol

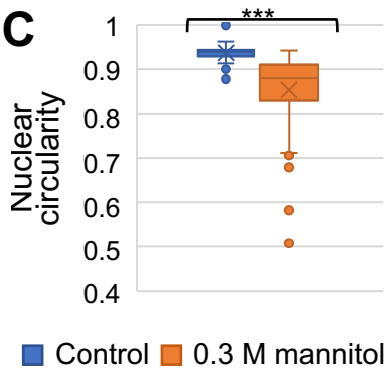
C
Nuclear circularity
1
0.9
0.8
0.7
0.6
0.5
0.4
***
Control
0.3 M mannitol

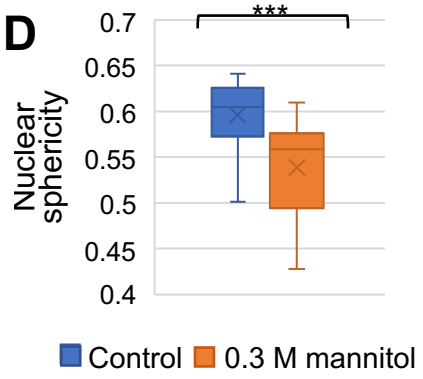
D
Nuclear sphericity
0.7
0.65
0.6
0.55
0.5
0.45
0.4
***
Control
0.3 M mannitol

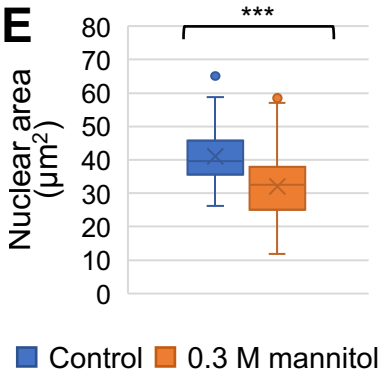
E
Nuclear area (μm²)
80
70
60
50
40
30
20
10
0
***
Control
0.3 M mannitol

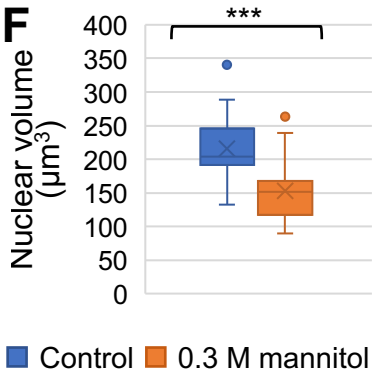
F
Nuclear volume (μm³)
400
350
300
250
200
150
100
50
0
***
Control
0.3 M mannitol

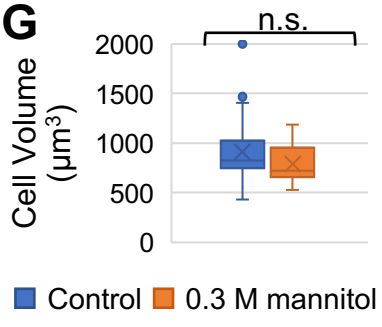
G
Cell Volume (μm³)
2000
1500
1000
500
0
n.s.
Control
0.3 M mannitol

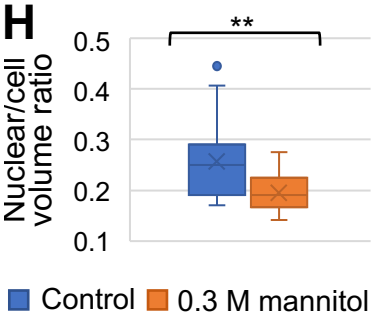
H
Nuclear/cell volume ratio
0.5
0.4
0.3
0.2
0.1
**
Control
0.3 M mannitol

Figure 2

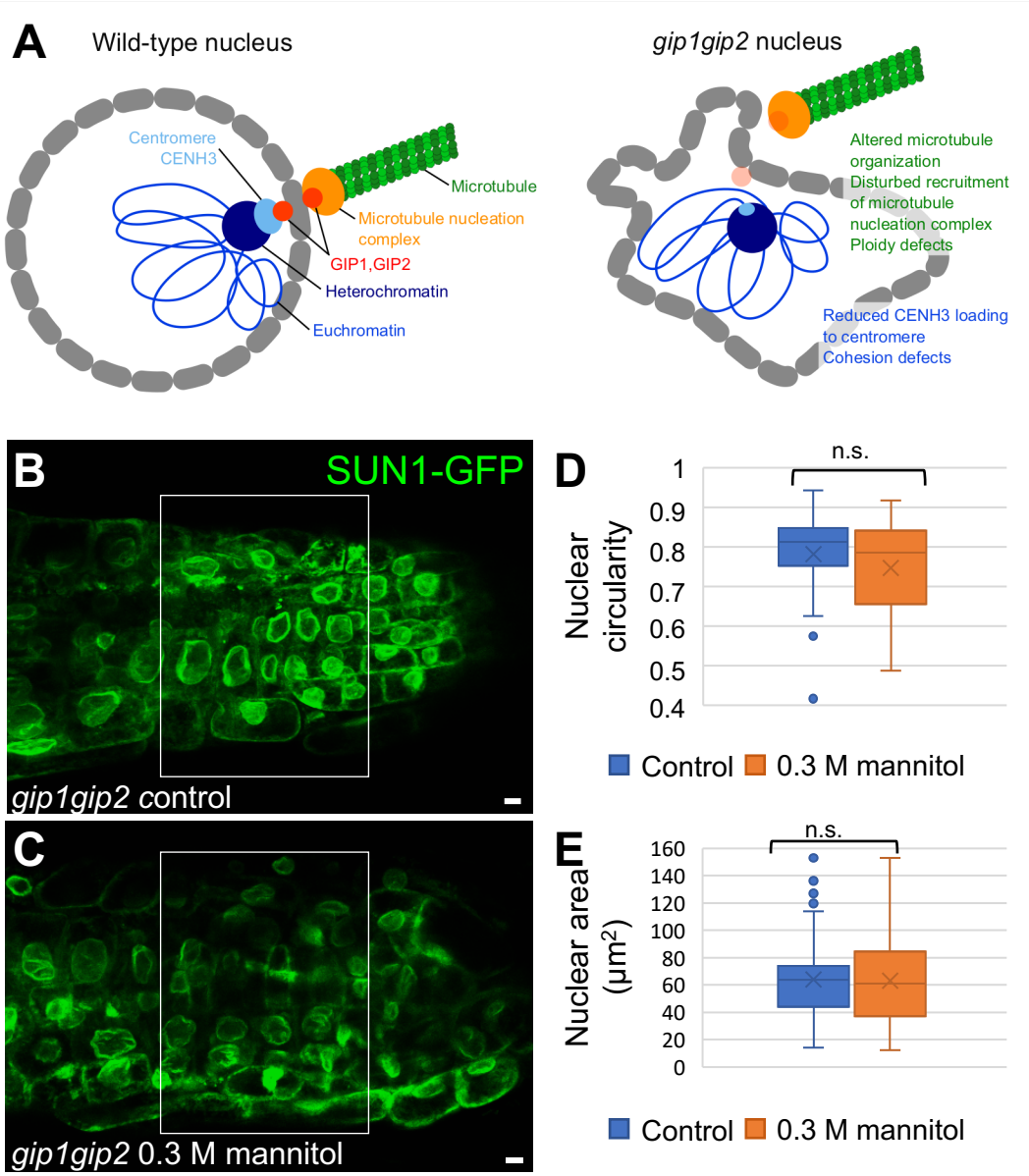
A
Wild-type nucleus
gip1gip2 nucleus
Centromere
CENH3
Microtubule
Microtubule nucleation complex
GIP1,GIP2
Heterochromatin
Euchromatin
Altered microtubule organization
Disturbed recruitment of microtubule nucleation complex
Ploidy defects
Reduced CENH3 loading to centromere
Cohesion defects
B
SUN1-GFP
gip1gip2 control
C
gip1gip2 0.3 M mannitol
D
n.s.
Nuclear circularity
1
0.9
0.8
0.7
0.6
0.5
0.4
Control
0.3 M mannitol
E
n.s.
Nuclear area (µm²)
160
140
120
100
80
60
40
20
0
Control
0.3 M mannitol

Figure 3

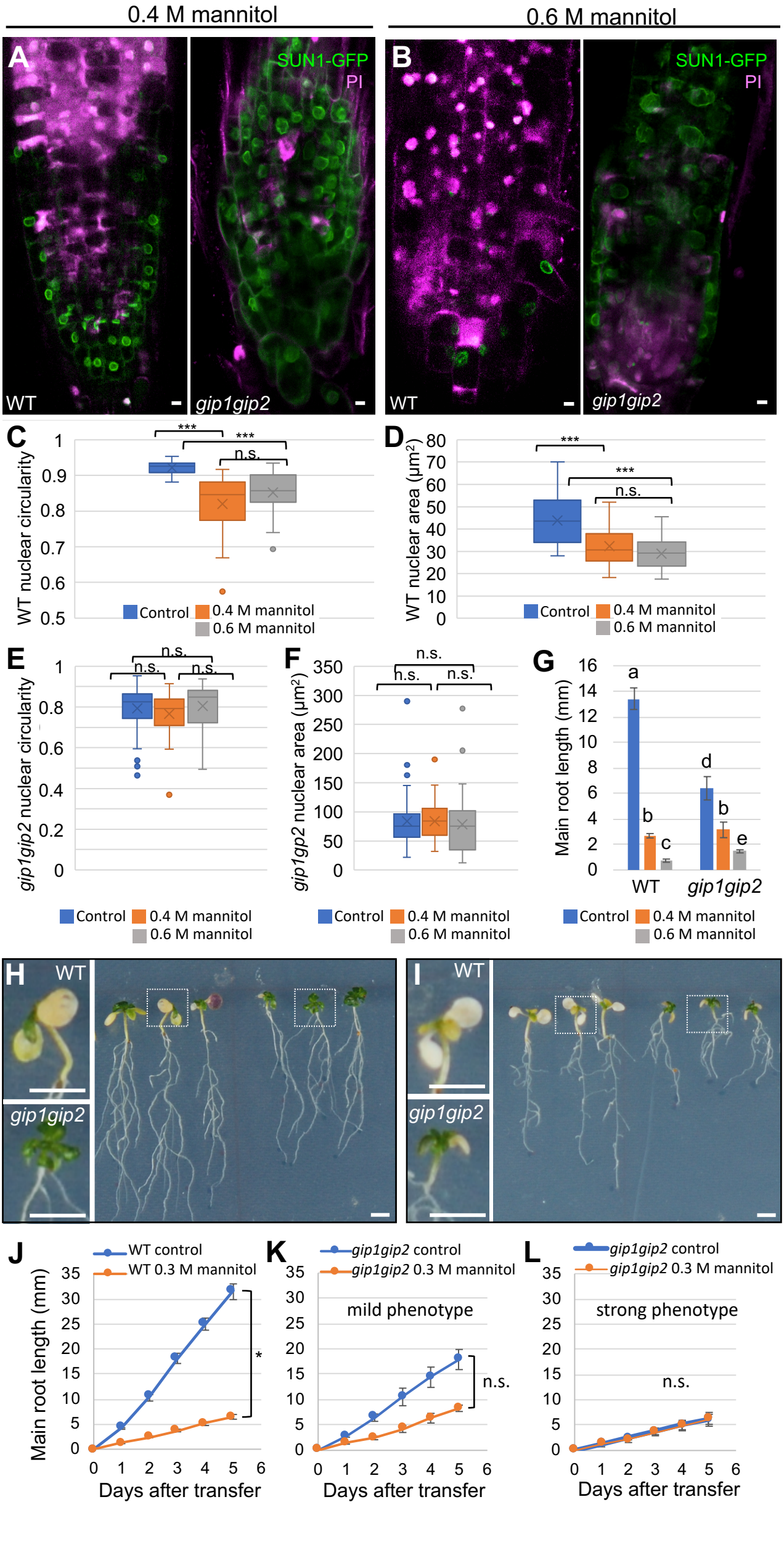
0.4 M mannitol
0.6 M mannitol
A
B
SUN1-GFP
PI
WT
gip1gip2
C
WT nuclear circularity
***
n.s.
D
WT nuclear area (µm²)
E
gip1gip2 nuclear circularity
F
gip1gp2 nuclear area (µm²)
G
Main root length (mm)
a
b
c
d
e
Control
0.4 M mannitol
0.6 M mannitol
H
I
J
WT control
WT 0.3 M mannitol
Days after transfer
K
gip1gip2 control
gip1gip2 0.3 M mannitol
mild phenotype
L
strong phenotype

Figure 4

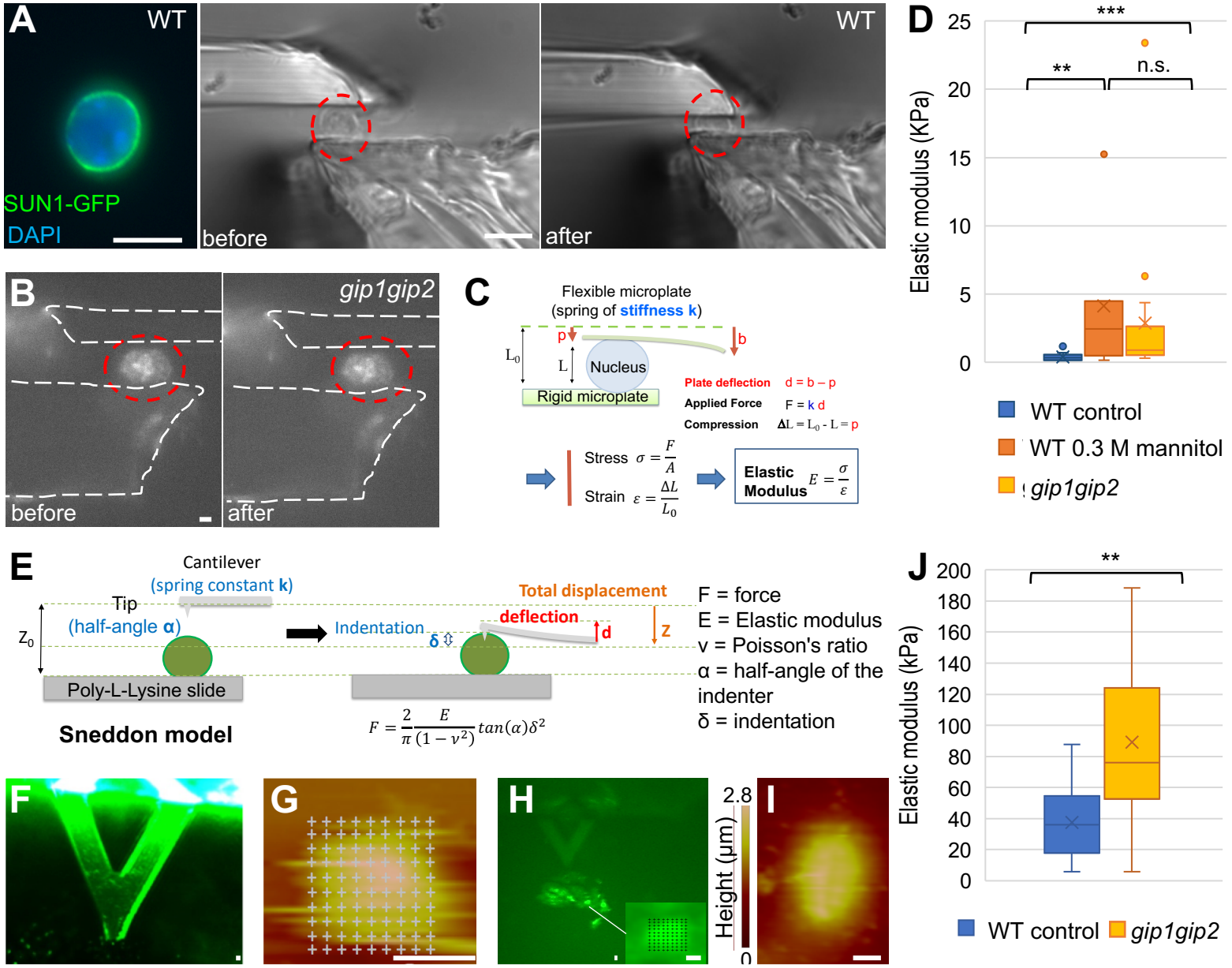
A
WT
SUN1-GFP
DAPI
before
after
WT
B
gip1gip2
before
after
C
Flexible microplate
(spring of stiffness k)
p
b
L0
L
Nucleus
Rigid microplate
Plate deflection d = b – p
Applied Force F = k d
Compression ΔL = L0 - L = p
Stress σ = F/A
Strain ε = ΔL/L0
Elastic Modulus E = σ/ε
D
Elastic modulus (KPa)
25
20
15
10
5
0
***
**
n.s.
WT control
WT 0.3 M mannitol
gip1gip2
E
Cantilever
(spring constant k)
Tip
(half-angle α)
Z0
Indentation
δ
Total displacement
deflection
d
z
Poly-L-Lysine slide
Sneddon model
F = force
E = Elastic modulus
v = Poisson's ratio
α = half-angle of the indenter
δ = indentation
J
Elastic modulus (kPa)
200
180
160
140
120
100
80
60
40
20
0
**
WT control
gip1gip2
F
G
H
Height (μm)
2.8
0
I

Figure 5

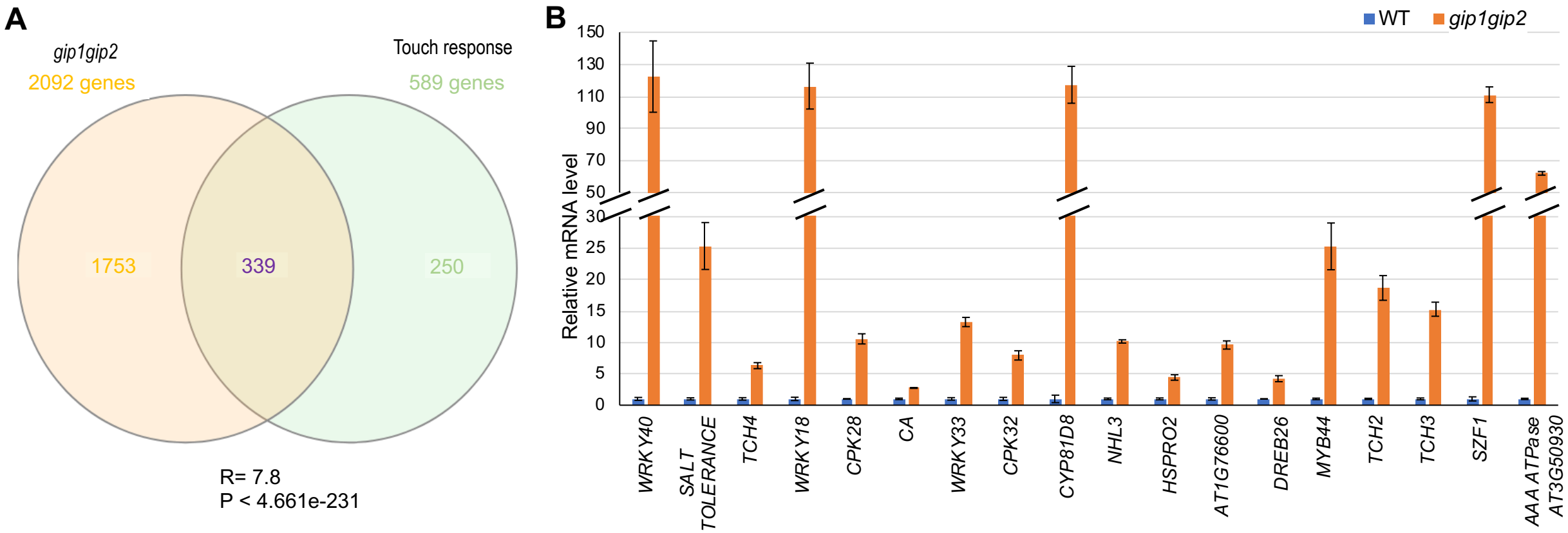
A
gip1gip2
2092 genes
Touch response
589 genes
1753
339
250
R= 7.8
P < 4.661e-231
B
WT
gip1gip2
Relative mRNA level
150
130
110
90
70
50
30
25
20
15
10
5
0
WRKY40
SALT TOLERANCE
TCH4
WRKY18
CPK28
CA
WRKY33
CPK32
CYP81D8
NHL3
HSPRO2
AT1G76600
DREB26
MYB44
TCH2
TCH3
SZF1
AAA ATPase AT3G50930

Figure 6

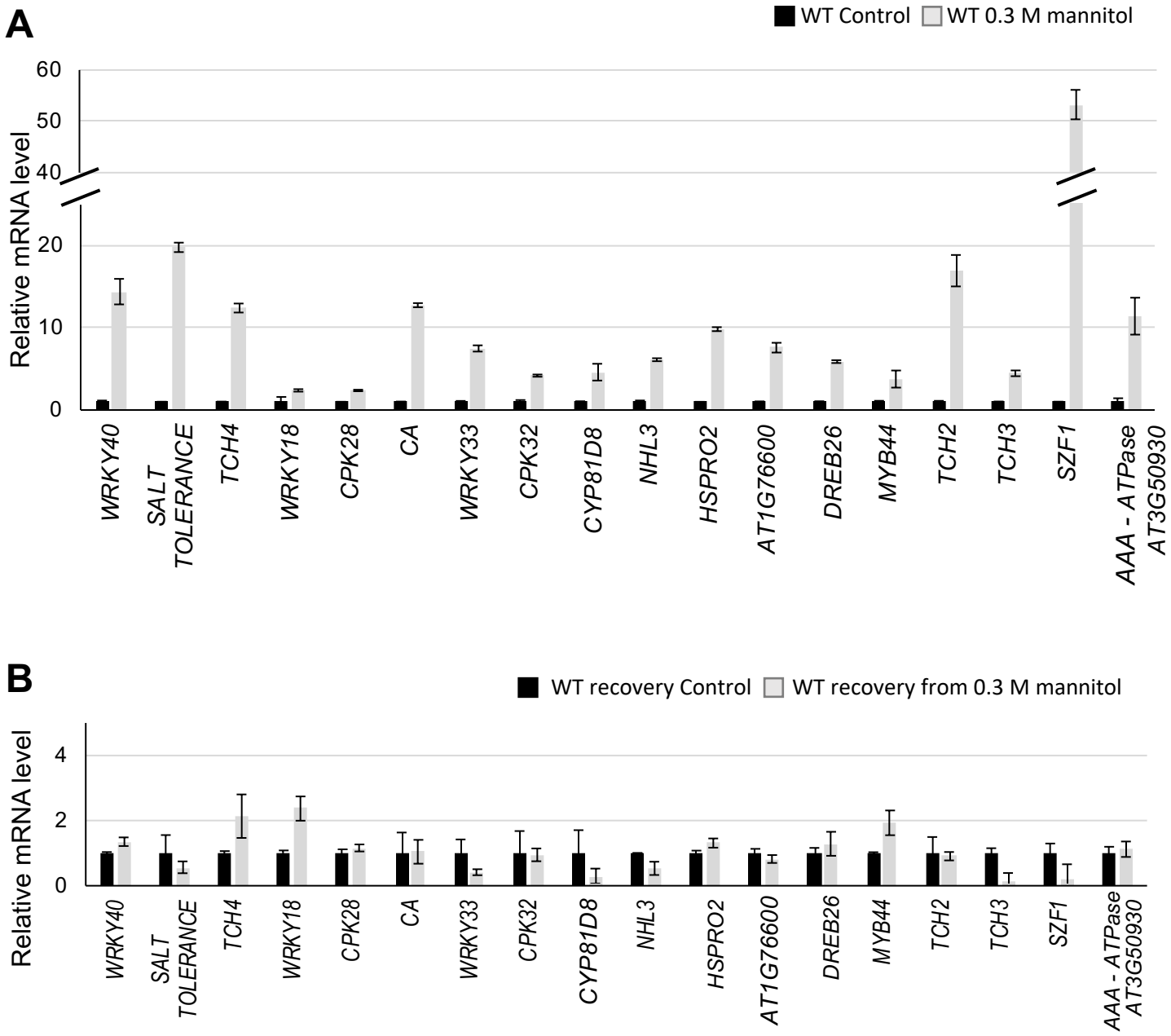
A
WT Control
WT 0.3 M mannitol
Relative mRNA level
60
50
40
20
10
0
WRKY40
SALT TOLERANCE
TCH4
WRKY18
CPK28
CA
WRKY33
CPK32
CYP81D8
NHL3
HSPRO2
AT1G76600
DREB26
MYB44
TCH2
TCH3
SZF1
AAA - ATPase AT3G50930
B
WT recovery Control
WT recovery from 0.3 M mannitol
Relative mRNA level
4
2
0
WRKY40
SALT TOLERANCE
TCH4
WRKY18
CPK28
CA
WRKY33
CPK32
CYP81D8
NHL3
HSPRO2
AT1G76600
DREB26
MYB44
TCH2
TCH3
SZF1
AAA - ATPase AT3G50930

Figure 7

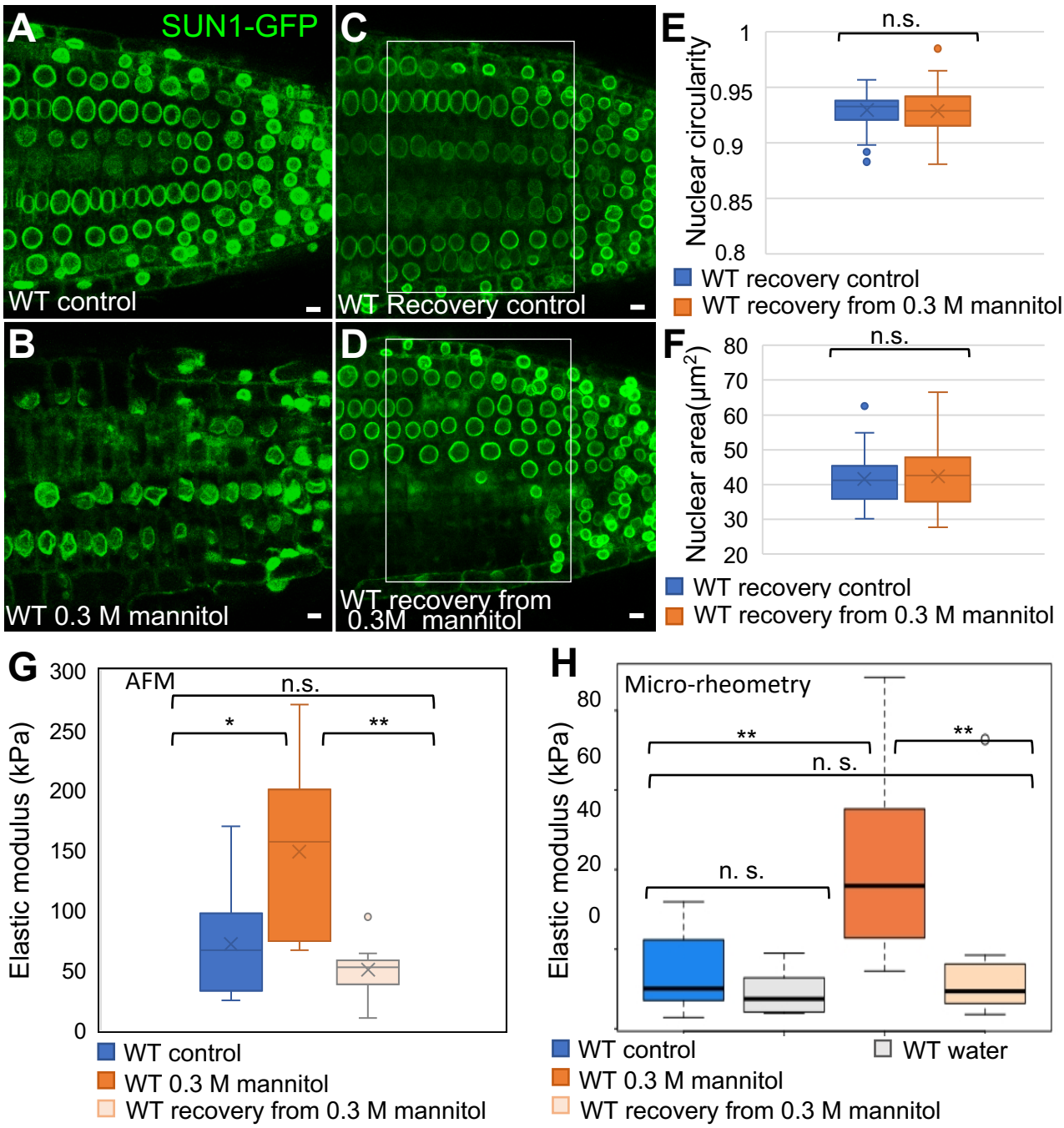
A
SUN1-GFP
WT control
B
WT 0.3 M mannitol
C
WT Recovery control
D
WT recovery from 0.3M mannitol
E
n.s.
Nuclear circularity
1
0.95
0.9
0.85
0.8
WT recovery control
WT recovery from 0.3 M mannitol
F
n.s.
Nuclear area(μm²)
80
70
60
50
40
30
20
WT recovery control
WT recovery from 0.3 M mannitol
G
AFM
n.s.
*
**
Elastic modulus (kPa)
300
250
200
150
100
50
0
WT control
WT 0.3 M mannitol
WT recovery from 0.3 M mannitol
H
Micro-rheometry
**
**
n. s.
n. s.
Elastic modulus (kPa)
80
60
40
20
0
WT control
WT water
WT 0.3 M mannitol
WT recovery from 0.3 M mannitol
I
osmolarity
Nuclear shape : Expansion
Nuclear stiffness : Softening?
Shrinking
Stiffening
Nucleus
(isolated)
Hypo-osmotic
stress
Nucleus
Hyper-osmotic
stress
Recovery
Nucleus
Touch gene
expression
-
+
Nuclear envelope
GIP
Plant growth sensitivity
to hyperosmotic stress

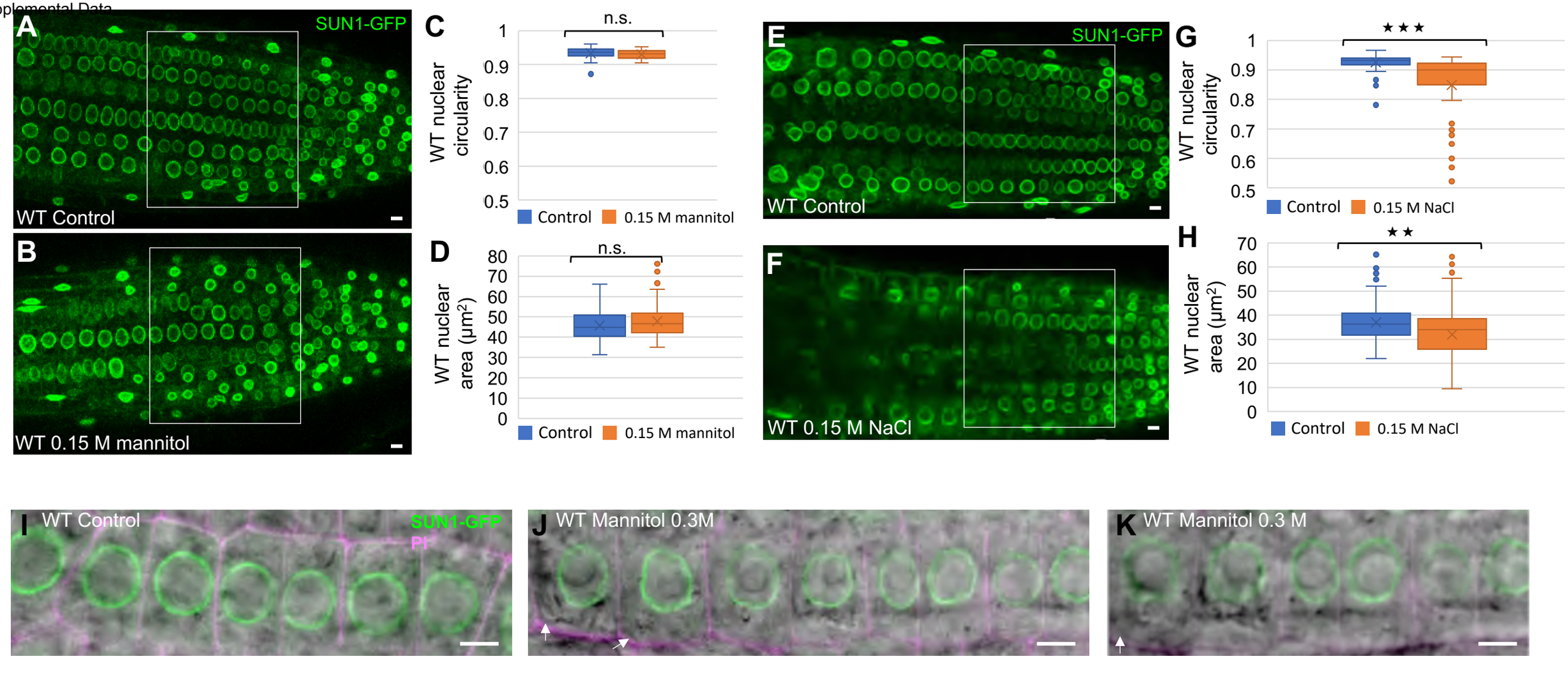

Figure S1. Cell and nuclear shape analysis in root meristems under various osmotic conditions related to Figure 1 : (A-D) in the presence of 0.15 M mannitol (A-B) Representative images of root meristems of 9-day-old seedlings expressing SUN1-GFP in absence (A) or presence (B) of 0.15 M mannitol (16h-treatment). Scale bars are 5 µm. (C-D) Quantification of the nuclear circularity (C) and area (D). The *p*-values after Student's t-test are 0.163 and 0.168, respectively, indicating no significant nuclear changes after 0.15 M mannitol treatment (n.s.). $n_{control} = 54$; $n_{treated} = 57$. (E-H) in the presence of 0.15 M NaCl. (E-F) Representative images of root meristems of 9-day-old seedlings expressing SUN1-GFP in absence (E) or presence (F) of 0.15 M NaCl (16h-treatment). Scale bars are 5 µm. (G-H) Quantification of the nuclear circularity (G) and area (H). Using Student's t –test, the *p*-values are 1.9e-8 and 0.0043, respectively, indicating significant changes (***$p \leq 0.001$, **$p \leq 0.01$, respectively). $n_{control} = 91$ and $n_{treated} = 51$. (I-K) in presence of 0.3 M mannitol. Representative images of root meristems of 9-day-old seedlings expressing SUN1-GFP in absence (I) or presence (J-H) of 0.3 M mannitol (16h-treatment). Merge are presented combining DIC and fluorescent channels (GFP, green, for NE, and PI, magenta, for cell wall). White arrows indicate plasma membrane detachment in a few cells. Scale bars are 5 µm.

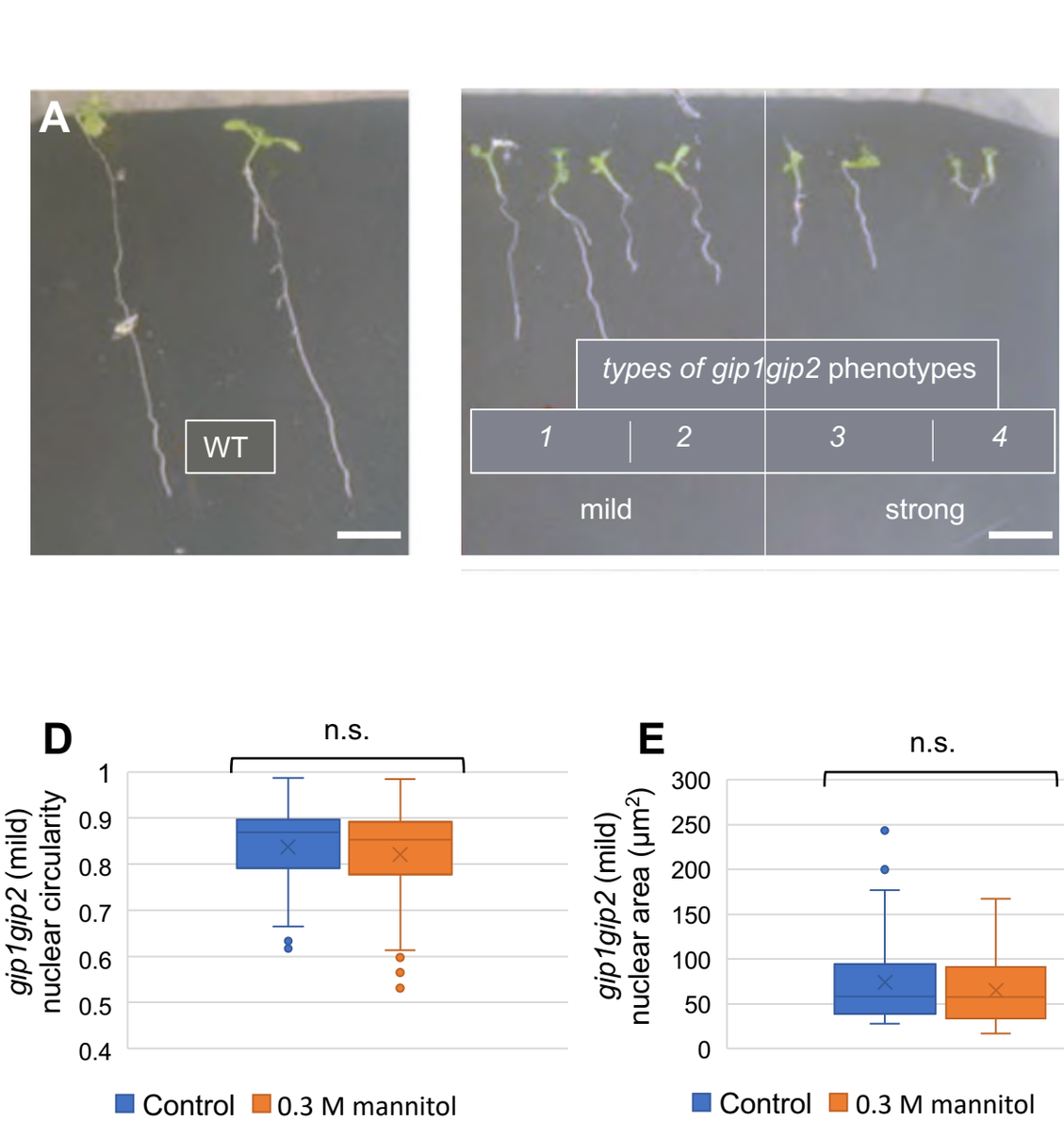

Figure S2. Characterization of the *gip1gip2* mutant, related to Figure 2: (A) Nine days-old-seedlings : mild (type 1-2) and severe (type 3-4) phenotypes of the *gip1gip2* mutant can be distinguished from WT based on the length of their main root. Scale bar is 0.5 cm (B-E) Nuclear shape analysis in root meristems of mild *gip1gip2* phenotype in the presence of 0.3 M mannitol (B-C). Representative images of root meristems of 9-day-old seedlings expressing SUN1-GFP in absence (B) or presence (C) of 0.3 M mannitol (16h-treatment). Scale bars are 5 µm. (D-E) Quantification of nuclear circularity (D) and area (E). The *p*-values after Student's t-test are 0.34 and 0.24, indicating no significant nuclear changes after 0.3M mannitol treatment (n.s.). $n_{control} = 55$ and $n_{treated} = 62$ (F) Nuclear area was evaluated in flow sorted nuclei isolated from root of WT and mild *gip1gip2* phenotype as described in [S1]. Using a Student's t-test significant difference was obtained between $2C_{WT}$ nuclei (n = 18) and $2C_{gip1gip2}$ nuclei (n =19), *p*-value 0.0014 (*).

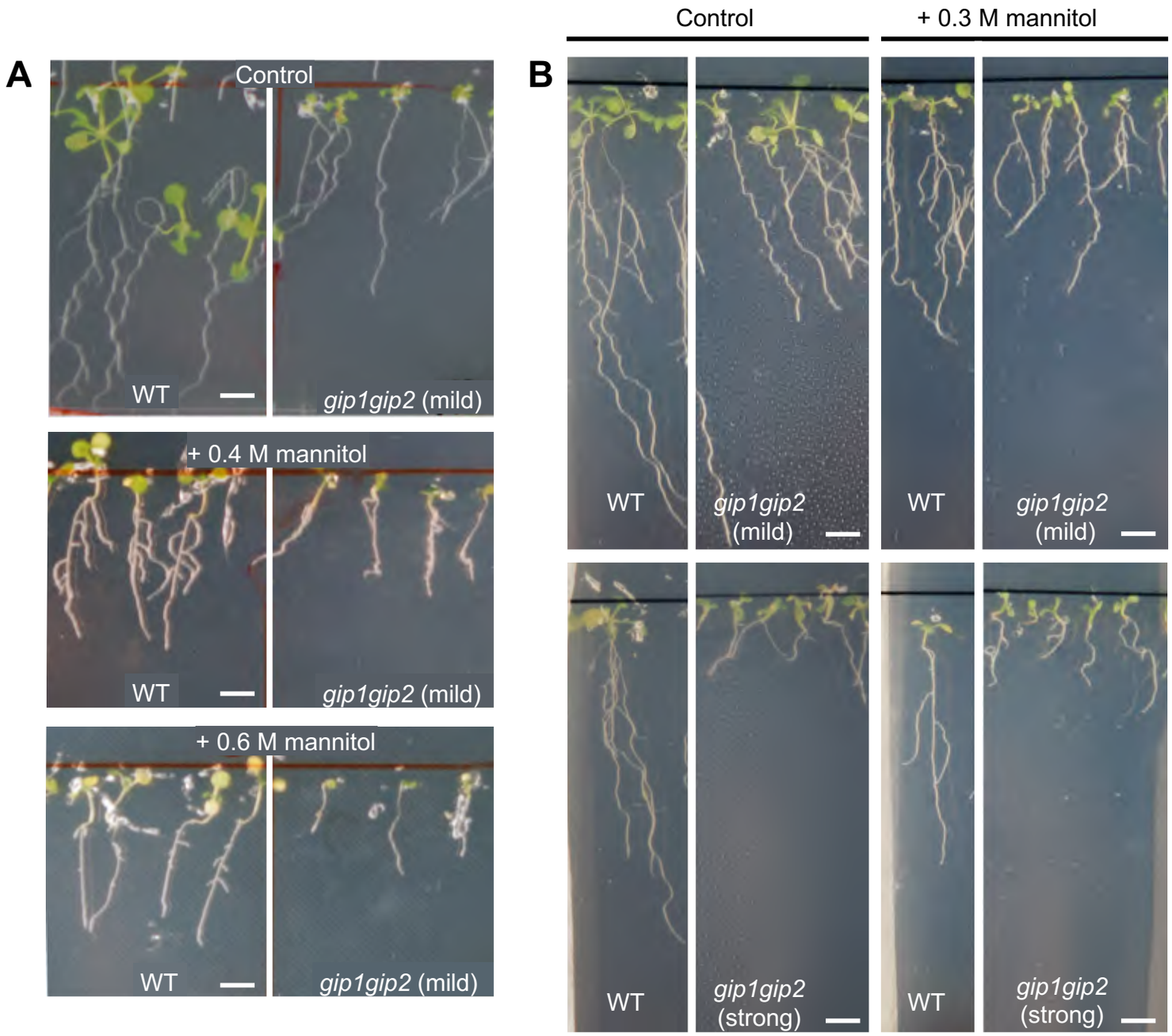

Figure S3. Phenotype of the *gip1gip2* mutant and WT seedlings in presence of various mannitol concentrations, related to Figure 3. (A) mild *gip1gip2* phenotype and WT 9-day-old seedlings grown in normal conditions were transferred on control, or 0.4 and 0.6M mannitol media and observed after 2 days. (B) mild and strong *gip1gip2* and WT 9-day-old seedlings were transferred on 0.3 M mannitol and control media and observed after 5 days. Scale bars are 0.5 cm.

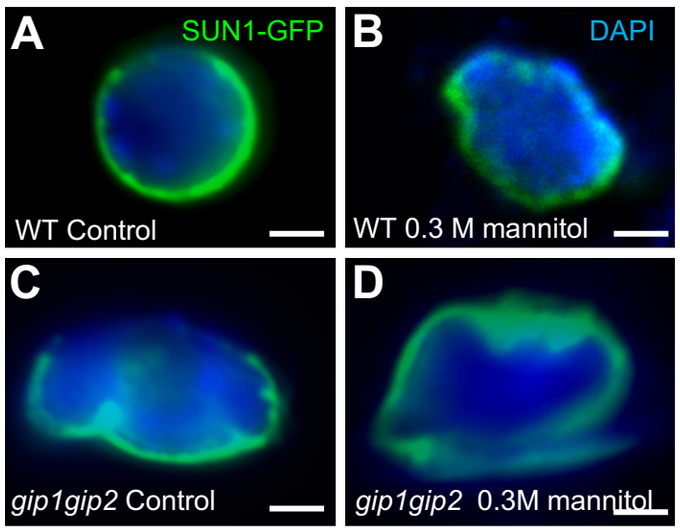

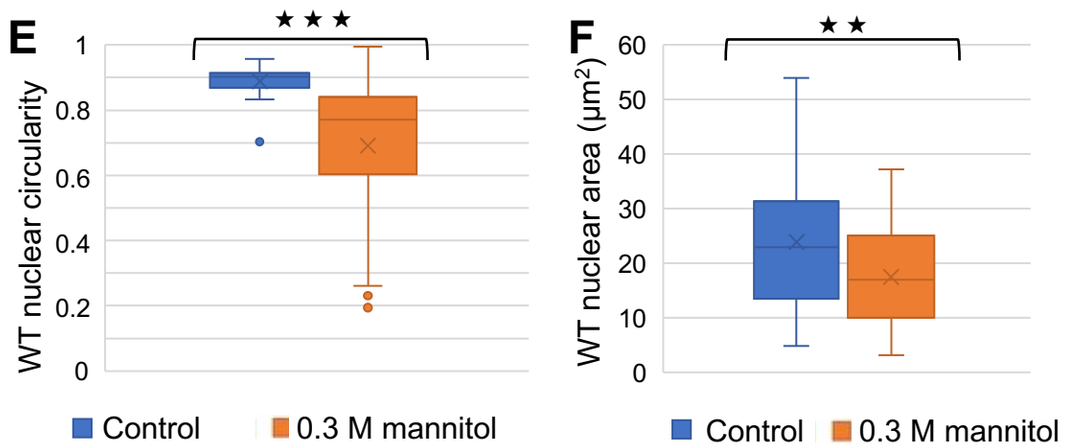

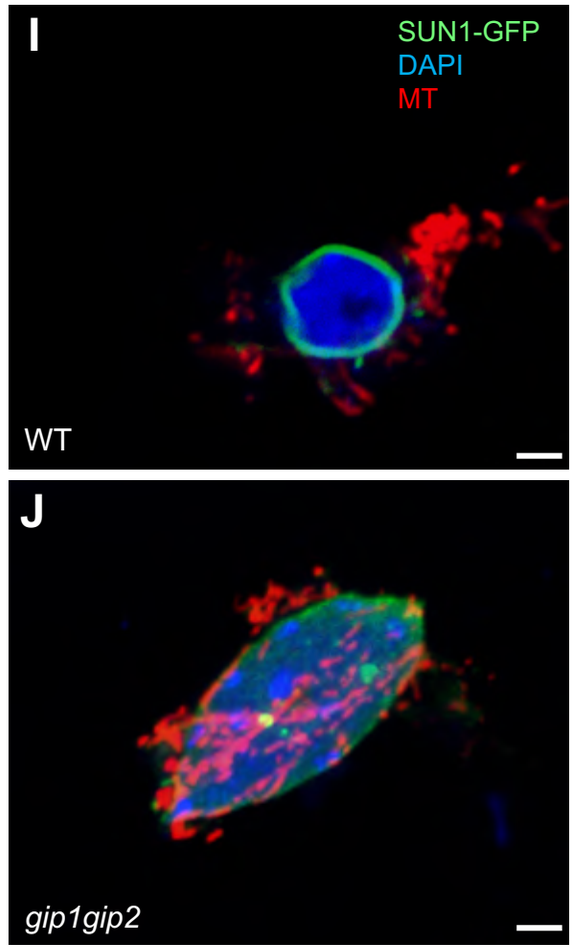

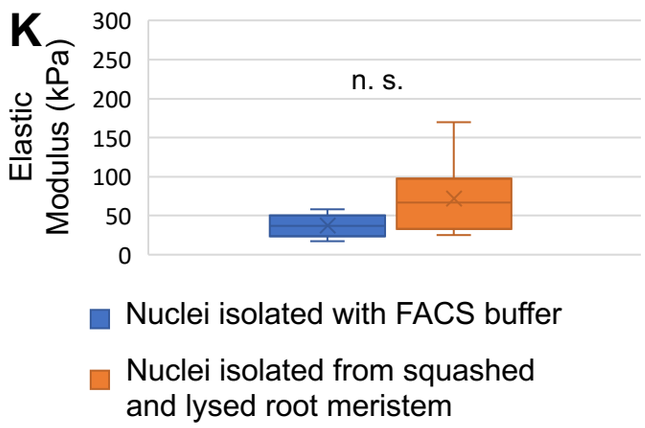

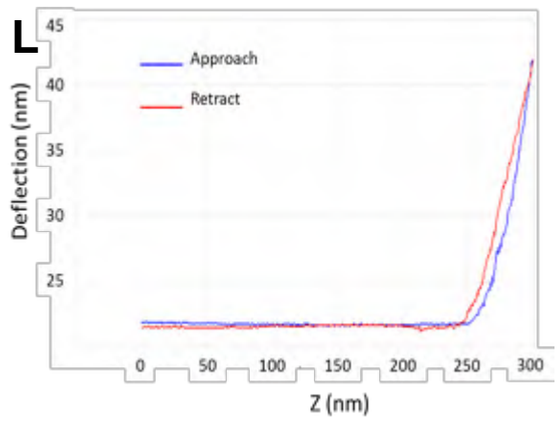

$F = kd$
Applied force

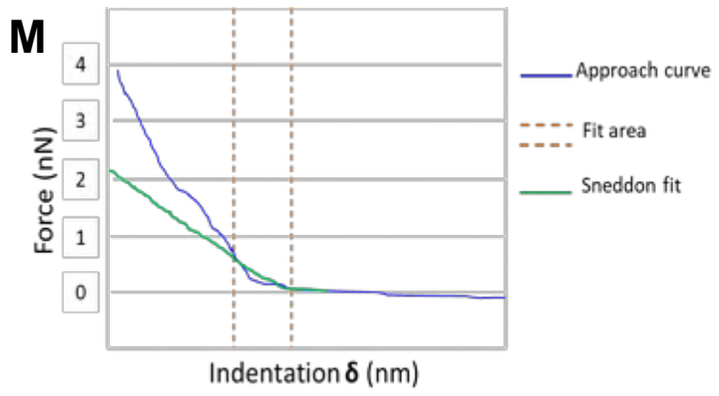

Figure S4. Characterization of nuclei used for nuclear rigidity measurements, related to Figure 4. (A-D) Nuclei were isolated from root tips using FACS buffer in presence of DAPI. Experiments were performed on 9-day-old seedlings expressing SUN1-GFP in WT control (n = 33) (A) and WT treated with 0.3 M mannitol (n = 57) (B) as well as in *gip1gip2* control (n =34) (C) and *gip1gip2* treated with 0.3 M mannitol (n = 53) (*D*). Scale bars are 2 µm. (E-H) Nuclear circularity (E-G) and nuclear area (F-H) were quantified. Using Student's t-test, significant differences were observed between WT control and WT 0.3M mannitol for nuclear circularity and area, respectively, with *p* values of 2.7e-9 (***) and 0.0079 (**); but not for *gip1gip2* with *p* values of 0.94 and 0.083, respectively (n.s.). (I-J) Immunostaining with anti-tubulin antibody performed on isolated nuclei from 9-day-old seedlings expressing SUN1-GFP in WT (I) and *gip1gip2* (J), as used in micro-rheometry experiments. Fixation and immunostaining were performed as described in [S1]. Scale bars, 2 µm. (K) AFM measurements comparing the elastic moduli of isolated nuclei as used in micro-rheometry (n = 5) to those of nuclei from squashed root meristems AFM (n = 6). Using Mann Whitney test no significant difference was observed (n.s.) with a *p* value of 0.193. (L-M) AFM measurements details. Calibration of the AFM probe with approach (blue) and retraction (red) (L). (M) Example of a force-indentation curve for one nucleus.

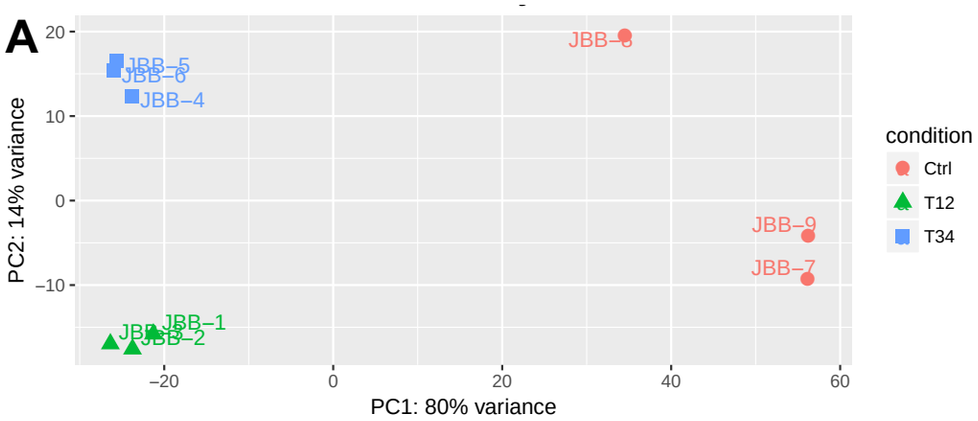

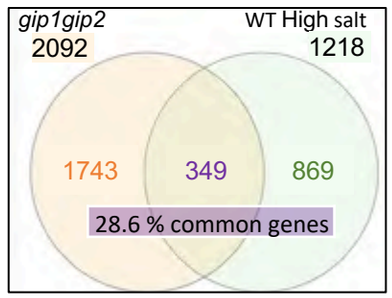

Representation factor: 3.9
p < 3.704e-67

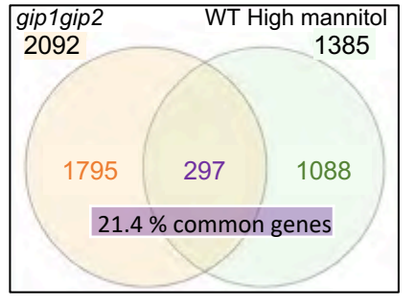

Representation factor: 2.9
p < 2.904e-118

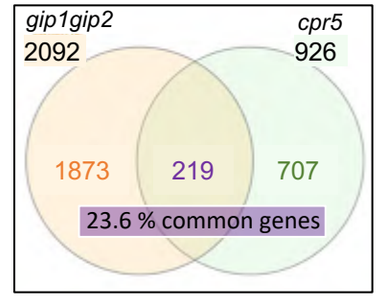

Representation factor: 3.2
p < 9.703e-57

E

Accession number	Genes	Description	log 2 fold change in mild phenotype *gip1gip2*	log 2 fold change in strong phenotype *gip1gip2*	fold change in the touch response
AT5G37770	*TOUCH2 (TCH2)*	Encodes CaM-like proteins (CML24)	2.41	2.52	6.55
AT2G41100	*TOUCH3 (TCH3)*	Encodes CaM-like proteins (CML12)	3.86	3.80	2.37
AT5G57560	***TOUCH4 (TCH4)***	Encodes a xyloglucan endotransglucosylase/hydrolase	1.24	1.73	21.17
AT4G31800	***WRKY family transcription factor (WRKY18)***	Pathogen-induced transcription factor	4.06	4.61	19.56
AT2G38470	*WRKY family transcription factor (WRKY33)*	Pathogen-induced transcription factor	1.86	2.74	12.39
AT1G80840	***WRKY family transcription factor (WRKY40)***	Pathogen-induced transcription factor	5.14	5.81	43.1
AT1G27730	***Salt tolerance zinc finger (Salt tolerance)***	Transcriptional repressor, Involved in response to several abiotic stresses	3.29	4.49	29.4
AT5G66210	*Calcium-dependent protein kinase (CPK28)*	Abscisic acid-activated signalling pathway	2.11	2.61	13.07
AT3G57530	*Calcium-dependent protein kinase (CPK32)*	Abscisic acid-activated signalling pathway	1.50	1.92	11.50
AT4G27280	*Calcium-binding EF-hand family protein (CA)*	Response to karrikin	2.43	3.09	12.68
AT3G50930	***AAA-type ATPase family (AAA)***	Involved in cell death	3.50	4.26	10.69
AT3G55980	*SZF1*	Transcription factor, involved in Chitin response	3.19	3.96	18.7
AT1G76600	*A2 unknown function*	Unknown function	1.67	2.08	10.51
AT1G21910	*DREB26*	Transcription factor, encodes an AP2 type	1.60	1.13	4.07
AT5G67300	*Myb44*	Transcription factor, involved in mediating plant responses to several abiotic stresses	2.32	2.56	5.35
AT4G37370	***CYP81D8***	Encodes cytochrome P450 family proteins	1.44	1.88	2.26
AT5G06320	*NHL3*	Positive regulator of plant defense	1.86	2.63	3.34
AT2G40000	***HSPRO2***	Encodes salicylic acid-responsive positive regulator of basal resistance	1.36	1.82	18.5

Figure S5. Transcriptomic analyses of the *gip1gip2* mutant, related to Figure 5. (A) PCA analysis of the samples used for the transcriptome study to confirm that the 9 samples cluster correctly according to their genotype (DESeq2 package), *i.e.* in 3 groups WT and two populations (T12, mild phenotype and T34, strong phenotype) of *gip1gip2* mutants. (B-D) A list of genes found up-regulated in both mild and severe *gip1gip2* phenotypes was established. Venn diagrams show the overlap between up-regulated genes in *gip1gip2,* WT high salt (B), WT high mannitol (C) and *cpr5* (D) respectively [S2, S3]. The pourcentage of common genes are indicated as well as the representative factor. Statistical significance of the overlap is determined by the exact hypergeometric test (P is indicated) (E) Comparison of the fold change difference in expression for genes analyzed in the hyperosmotic stress response and in *gip1gip2* (mild and strong phenotypes). Bold genes are upregulated in high hyperosmotic conditions (salt, mannitol), and none of the 18 genes are found up regulated in *cpr5*.

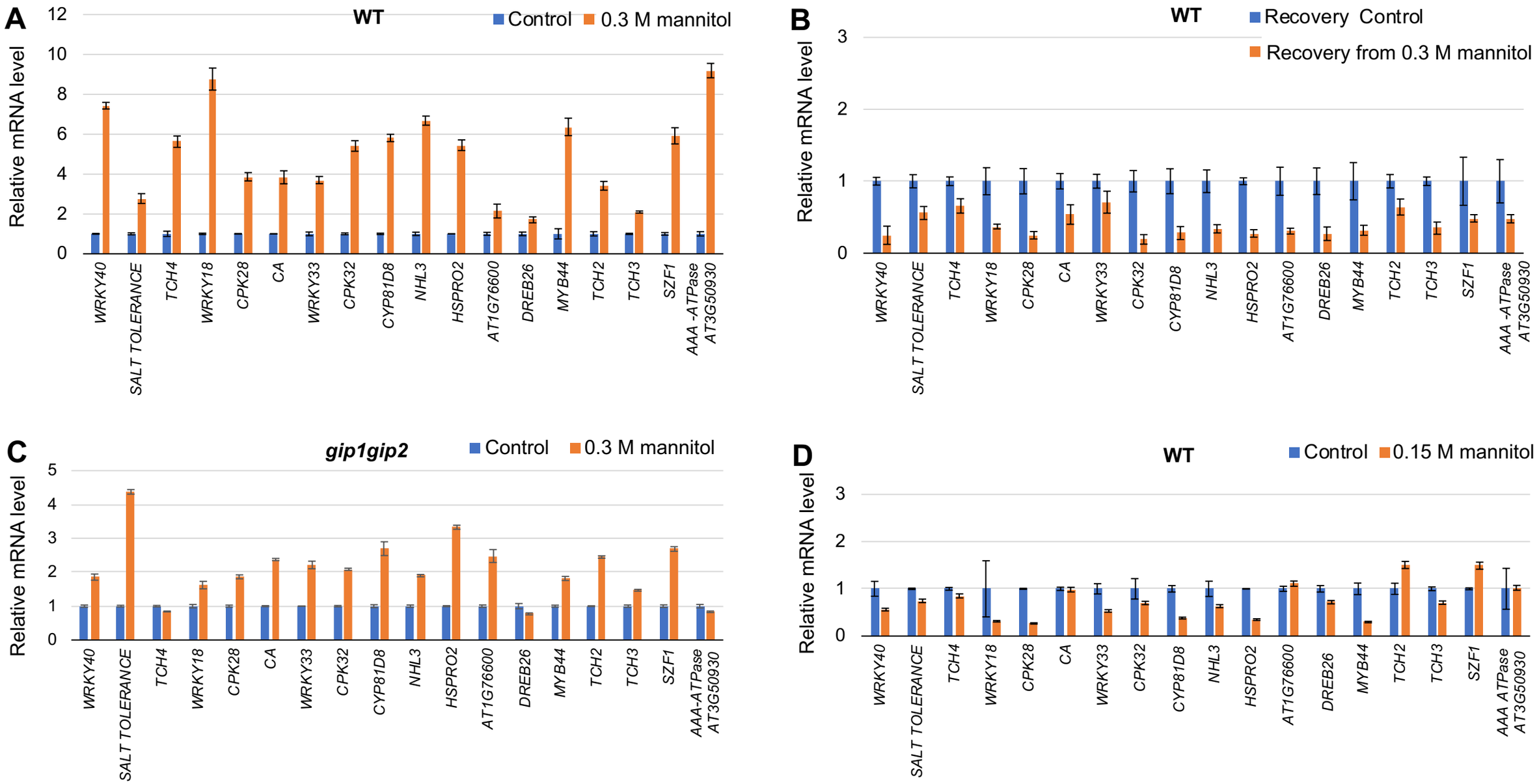

Figure S6. Relative mRNA level of touch induced genes in response to various osmotic stresses, related to Figure 6. (A) RNA was extracted from WT root seedlings treated with 0.3 M mannitol for 16 hours and in control conditions. (B) RNA was extracted from WT root seedlings treated with 0.3 M mannitol for 16 hours followed by 7hours of recovery in normal growth conditions. (C) RNA was extracted from 9-day-old *gip1gip2* seedlings treated with 0.3 M mannitol for 16 hours and control conditions. (D) RNA was extracted from 9-day-old WT seedlings treated with 0.15 M mannitol for 16 hours and control conditions. All the experiments were performed with 3 technical replicates and 2 biological replicates. SDs are indicated.

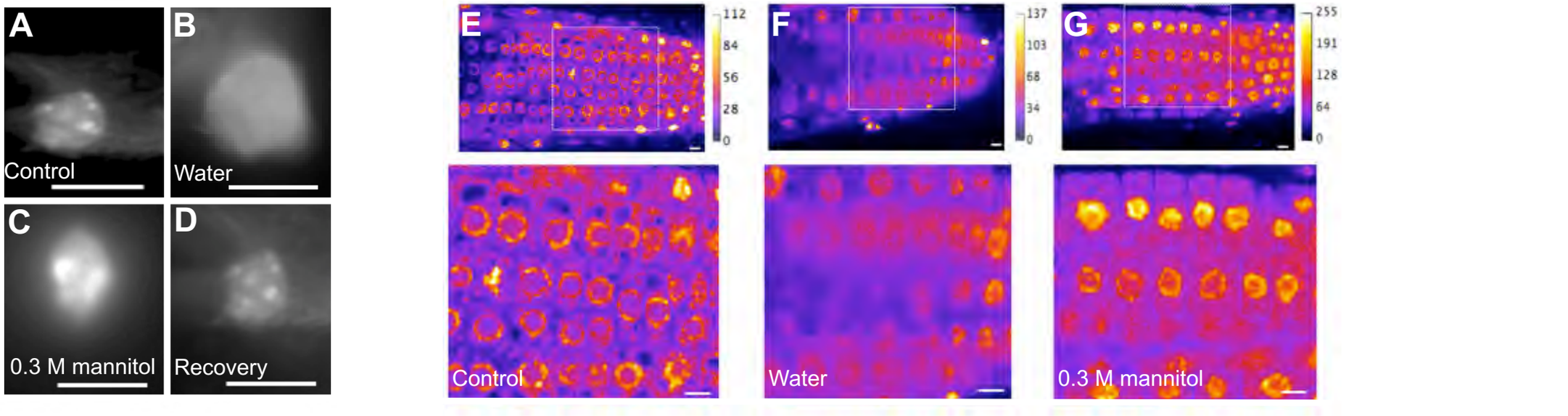

Figure S7. Analysis of nucleus and transcriptional responses to various osmotic stresses, related to Figure 7. (A-D) Representative fluorescence images of isolated nuclei compressed between parallel plates during micro-rheometry mechanical measurements. Nuclei were isolated from root tips of seedlings in control conditions using FACS buffer in presence of DAPI (A, n = 7), or after a 16h-water treatment (B, n = 5) compared to a 16h-0.3M mannitol treatment (C, n = 11) and recovery from 0.3 M mannitol (D, n = 8). Scale bars are 5 µm. (E-G) Nuclei in root tips of seedlings in control conditions (E), or a 16h-water treatment (F) compared to a 16h - 0.3M mannitol treatment (G) using a 10 min incubation of the roots in FACS buffer in presence of DAPI. Images were adjusted to the same background level and signal intensity was color-coded using the ImageJ Fire lookup table. Calibration bar is indicated on the right side of each picture. Magnification of dotted square are presented below each picture. Scale bars are 5 µm. (H-L) Nuclear area was evaluated in isolated nuclei from root tips (H) of WT seedlings treated in control conditions (n = 45), or a 16h -water treatment (n = 32) and a significant difference was observed using Student's-t test with a p value of 9.06e-8 (***). Similar analyses were performed on nuclei in planta (I) in WT control (n =164) and water-treated WT seedlings (n = 174) as well as in mild phenotype gip1gip2 (K) ($n_{control}$ = 80 and $n_{treated}$ = 57) but no significant differences were observed for nuclear area with p-values of 0.4 and 0.361, respectively. Nuclear circularity was also not significantly modified by water treatment with a p-value of 0.12 for WT and 0.553 for gip1gip2 (M-N) Analysis of the transcriptional response of touch induced genes in seedlings after a 16h-water treatment compared to control conditions in WT (M) and in gip1gip2 (N). All the experiments were performed with 3 technical replicates and 2 biological replicates. SDs are indicated.

GO	Count	%	PValue	List Total	Pop Hits	Pop Total	Fold Enrichment	Bonferroni	Benjamini	FDR
single-organism cellular process	831	40,22	3,86E-15	1644	7640	18449	1,220614944	4,59E-13	4,59E-14	4,45E-12
response to stress	670	32,43	2,33E-91	1644	3697	18449	2,033744399	2,75E-89	2,75E-89	2,67E-88
single-organism metabolic process	610	29,53	1,75E-39	1644	4317	18449	1,585691886	2,07E-37	5,17E-38	2,01E-36
response to chemical	512	24,78	5,95E-62	1644	2884	18449	1,992258657	7,02E-60	3,51E-60	6,81E-59
response to abiotic stimulus	380	18,39	5,43E-51	1644	2004	18449	2,127927843	6,41E-49	2,14E-49	6,21E-48
cellular response to stimulus	342	16,55	6,16E-07	1644	3022	18449	1,269996908	7,27E-05	6,61E-06	7,05E-04
response to endogenous stimulus	303	14,67	8,66E-32	1644	1757	18449	1,935271427	1,02E-29	1,28E-30	9,91E-29
response to external stimulus	300	14,52	1,01E-36	1644	1631	18449	2,064136014	1,19E-34	1,70E-35	1,15E-33
response to biotic stimulus	258	12,49	5,19E-38	1644	1282	18449	2,258409533	6,12E-36	1,22E-36	5,94E-35
response to other organism	250	12,10	6,83E-38	1644	1224	18449	2,292079139	8,06E-36	1,34E-36	7,82E-35
immune response	89	4,31	9,50E-20	1644	351	18449	2,845469323	1,12E-17	1,24E-18	1,09E-16
regulation of response to stimulus	84	4,07	1,29E-05	1644	584	18449	1,614126087	0,00152201	1,17E-04	0,01477155
regulation of immune system process	28	1,36	8,92E-07	1644	110	18449	2,856514046	1,05E-04	8,77E-06	0,00102031
immune effector process	18	0,87	7,10E-05	1644	68	18449	2,970534564	0,00834467	5,98E-04	0,08123838
interspecies interaction between organisms	30	1,45	7,57E-05	1644	153	18449	2,200395973	0,00889146	5,95E-04	0,08658314
single organism signaling	230	11,13	1,80E-04	1644	2064	18449	1,250515735	0,02096223	0,00132319	0,20525504
single-organism localization	196	9,49	2,90E-04	1644	1735	18449	1,267732458	0,03366872	0,00201259	0,33161306
positive regulation of response to stimulus	32	1,55	0,00100479	1644	194	18449	1,851054757	0,11185862	0,00656857	1,14390069
hormone metabolic process	28	1,36	0,00131436	1644	164	18449	1,915954543	0,14375262	0,00813494	1,49391672
multi-organism cellular process	25	1,21	0,00574709	1644	156	18449	1,798400555	0,49344035	0,03343397	6,38332439
positive regulation of immune system process	13	0,63	0,00683841	1644	61	18449	2,391577919	0,55501016	0,03782345	7,55258371
regulation of multi-organism process	18	0,87	0,01023072	1644	104	18449	1,9422726	0,70282758	0,05366295	11,1026025
seed oilbody biogenesis	4	0,19	0,01876494	1644	7	18449	6,412582551	0,89304021	0,09261374	19,4903947
negative regulation of circadian rhythm	3	0,15	0,02236962	1644	3	18449	11,22201946	0,93071916	0,10526956	22,8110096
maintenance of location	12	0,58	0,03701776	1644	68	18449	1,980356376	0,98833306	0,16309094	35,0586522
cell wall organization or biogenesis	81	3,92	0,04106787	1644	742	18449	1,225045252	0,99290473	0,17330568	38,1167058
detection of stimulus	16	0,77	0,04524346	1644	105	18449	1,710022014	0,99576033	0,18318558	41,1314032
activation of immune response	8	0,39	0,05418344	1644	39	18449	2,301952711	0,99860294	0,2092423	47,1402537
circadian rhythm	17	0,82	0,05904587	1644	118	18449	1,616731618	0,99923954	0,21935975	50,1681252
negative regulation of response to stimulus	22	1,06	0,06083046	1644	165	18449	1,496269262	0,99939216	0,21874455	51,239082
protein folding	37	1,79	0,08717799	1644	320	18449	1,297546001	0,99997884	0,29333818	64,7918325

Table S1. GO annotations of biological functions linked to the most upregulated genes, related to Figure 5, in the *gip1gip2* transcriptome when compared to WT. In red are GO with FDR < 0.05

Genes	AGI Code	Forward primer	Reverse Primer
TCH2	AT5G37770	GTCGACGGTGATGATTCGTA	CATCAATCACCACATACTTCTAGGG
TCH3	AT2G41100	GGAATCTTTCAGGTTATTCGACA	AGGGAAAACATCACGGTACG
TCH4	AT5G57560	CCATGT TGTTCCAGGTGATTTCAAG	CCTCTGGTTCTGGATTCAAC
WRKY family transcription factor (*WRKY18*)	AT4G31800	CATCGGACACAAGCTTGACAGTT	TGCGCTGCGTTGTACCTTC
WRKY family transcription factor (*WRKY33*)	AT2G38470	GGGGACAATGAAACAAATGGTG	CGATTCTCGGCTCTCTCACTG
WRKY family transcription factor (*WRKY40*)	AT1G80840	CCAAGAGCTTACTTCAAATGTGC	CCTCCACACTTCTCTGAACCTT
Salt tolerance zinc finger (*SALT TOLERANCE*)	AT1G27730	ATCACACGTTTGCACCATCTG	CTTCGTAGTGGCACCGCT
Calcium-dependent protein kinase (*CPK28*)	AT5G66210	ATAACGCCTGAGGAACTTCG	TCCCATCTCTGTCTATGTCTGC
Calcium-dependent protein kinase (CPK32)	AT3G57530	GGGAAGCCTTGTCTGACGAAC	TGTTCCTGTTTTCATCATCGTTACAA
Calcium-binding EF-hand family protein (*CA*)	AT4G27280	TGTGTTGATGTTTAGGCTTAGCCC	TCCTCAATGACCTCCGTGACGA
AAA-type ATPase family (*AAA*)	AT3G50930	AGGTATTGAGGCGACAGAGG	ACAGAGTCATTTCTCATAAGCTGTTC
SZF1	AT3G55980	TCCAACTTTCTTCTCAATTTCATTC	TGTTAAGGTTCTTGAAGAGCAGAG
Unknown function (*A2*)	AT1G76600	GTCGCGATTGAGAAAGCAG	CGTCACAACCGGAGAGATTC
DREB26	AT1G21910	ACGATGCTCGATGAATACTTCTACG	TTAATTGAAACTCCAAAGCGGAATGTCAG
Myb44	AT5G67300	GCAACGTCATTGTCTCTCTCC	CAACTAGTACTGAGCTTAGCTTTAGGC
CYP81D8	AT4G37370	TCGTATCATTAAAGGAAACATGCTCGC	GGATGGTTCAACACGTTCGACAA
NHL3	AT5G06320	ACGGTGGTTGGAACTAAACTCG	TCCTCTCTCCGCCGTCAAG
HSPRO2	AT2G40000	TCATTTGCTTCAGGGGATG	CGCCACTAACTGCCTATACCC

Table S2. List of primers used in RT-qPCR experiments, related to Figures 5 and 6

Supplemental references:

[S1]: Batzenschlager, M., Lermontova, I., Schubert, V., Fuchs, J., Berr, A., Koini, M.A., Houlne, G., Herzog, E., Rutten, T., Alioua, A*., et al.* (2015). *Arabidopsis* MZT1 homologs GIP1 and GIP2 are essential for centromere architecture. Proc Natl Acad Sci U S A *112*, 8656-8660.
[S2]: Sewelam, N., Oshima, Y., Mitsuda, N., and Ohme-Takagi, M. (2014). A step towards understanding plant responses to multiple environmental stresses: a genome-wide study. Plant Cell Environ *37*, 2024-2035.
[S3]: Gu, Y., Zebell, S.G., Liang, Z., Wang, S., Kang, B.H., and Dong, X. (2016). Nuclear Pore Permeabilization Is a Convergent Signaling Event in Effector-Triggered Immunity. Cell *166*, 1526-1538 e1511.